ORNL/TM-1999/83

Advanced Industrial Materials (AIM) Program
Office of Industrial Technologies
Energy Efficiency and Renewable Energy
U.S. Department of Energy (DOE)

Advanced Industrial Materials (AIM) Program

Annual Progress Report

FY 1998

Date Published: May 1999

Coordinated by Peter Angelini
Compiled by Life Sciences Division
Oak Ridge National Laboratory

Prepared by the Oak Ridge National Laboratory
Oak Ridge, Tennessee 37831
for the U.S. Department of Energy
under contract number DE-AC05-96OR22464

TABLE OF CONTENTS

ADVANCED INTERMETALLICS/METALS AND COMPOSITES (continued)

NEW MATERIALS AND PROCESSES

NEW MATERIALS AND PROCESSES (continued)

POLYMERS

INTRODUCTION

Introduction to the Advanced Industrial Materials (AIM) Program
Office of Industrial Technologies
Fiscal Year 1998

C. A. Sorrell, Program Manager

The Advanced Industrial Materials (AIM) Program is in the Office of Industrial Technologies (OIT), Energy Efficiency and Renewable Energy, U.S. Department of Energy (DOE). The mission of AIM is to ?support development and commercialization of new or improved materials to improve energy efficiency, productivity, product quality, and reduced waste in the major process industries.? AIM investigators in the DOE national laboratories are working closely with approximately 100 companies via a range of mechanisms, including Cooperative Research and Development Agreements (CRADAs), User Centers, and informal partnerships. Research and development is being performed in a wide variety of materials technologies, including metallic and intermetallic alloys, ceramic and metal matrix composites, inorganic membrane materials, and coatings. The emphasis within AIM is on high-temperature, corrosion-resistant alloys and membrane materials; continuous fiber ceramic composites and monolithic ceramics are covered primarily by DOE's Continuous Fiber Ceramic Composites Program and Advanced Turbine Systems Program.

The Office of Industrial Technologies concentrates on the major process industries through the Industries of the Future (IOF) strategy. OIT has encouraged and assisted these industries in developing visions of what they will be like in 20 or 30 years, defining the drivers, technology needs, and barriers to realization of their visions. The visions provide a strategic framework for development of technology roadmaps and implementation plans. OIT then (1) provides cost-shared support for research and development to meet the needs identified in the roadmaps and (2) works with other governmental agencies to leverage resources. The Industries of the Future are agriculture, aluminum, chemicals, forest products, glass, metalcasting, mining, and petroleum refining. Other industries that serve the IOF industries also have stepped forward to develop visions and roadmaps and are ready to respond to solicitations of the IOF industries. These support industries are forging, heat treating, carbon products, and welding. The Portland cement industry recently has expressed a strong interest in following these examples.

In this context, the AIM Program supports the Industries of the Future by conducting research and development on materials to solve problems identified in the roadmaps. This work is done by national laboratory/industry/university teams with the facilities and expertise needed to develop new and improved materials. Each project in the AIM Program has active industrial participation and support.

In FY 1998, several projects were transferred to the IOF teams for further development and demonstration in industry. The zeolite membrane work at Sandia National Laboratories, New Mexico, under a CRADA with Amoco, is now supported by the

Chemical Industry budget, as is the electrochemical reactor work at Los Alamos National Laboratory, under a CRADA with Dow Chemical. The refractories work at Oak Ridge National Laboratory (ORNL) is now being supported by the Glass Industry budget, along with the molybdenum disilicide work at Los Alamos, under a CRADA with Johns Manville, and the chemical vapor deposition work at Sandia National Laboratory, California, under a CRADA with Pilkington Libby Owens Ford. Recently, the Los Alamos work on molybdenum disilicide and the Sandia work at the Combustion Research Facility have received funding directly from the Glass Industry budget resulting from a Laboratory solicitation. A new user facility for modeling the glass-melting furnace also was funded by the Glass Industry budget. The Steel Industry team has continued funding work on intermetallic alloys for the industry, based on the successful demonstration of steel transfer rolls by Bethlehem Steel. So the transfer of AIM-sponsored work to the IOF industries is beginning to work, and AIM is receiving due recognition from OIT management.

The designation of the Metals Processing Laboratory (MPLUS) at ORNL as a DOE User Center has been successful beyond our expectations. Over 80 proposals have been received, and many have been completed. Industry has been very enthusiastic about the opportunity to work at MPLUS and the other centers at ORNL. The Aluminum and Metal Casting teams are now providing funding for MPLUS, and others are likely to follow. The MPLUS business plan calls for referring potential users to other laboratories, with funding appropriate to the needs of the users. We are nearly at a funding level to make this work.

No brief summary can do justice to the quality and relevance of the work done by the hard-working AIM investigators. The reader will have to go through this entire volume to appreciate the magnitude of what has been accomplished with a relatively modest budget. It is not likely that many other government programs have produced so much for so little. The Program Manager expresses his appreciation for the support of such a fine group of people.

ADVANCED CERAMICS AND COMPOSITES

Advanced Manufacturing of Ceramics by Chemical Vapor Deposition Methods

M. D. Allendorf, A. H. McDaniel, and S. M. Ferko
Combustion Research Facility
Sandia National Laboratories
Livermore, California 94551-0969

INTRODUCTION

The objective of this project is to improve the efficiency and lower the cost of chemical vapor deposition (CVD) processes used to manufacture advanced ceramic materials by providing the physical and chemical understanding necessary to optimize and control these processes. Project deliverables include numerical process models, databases of thermodynamic and kinetic information related to the deposition process, and sensors and software algorithms that can be used for process control. Target manufacturing techniques include thin-film deposition processes used in the glass industry, CVD fiber-coating technologies (used to deposit interfacial coatings on continuous fiber ceramic preforms); chemical vapor infiltration; and coating techniques used to deposit wear-, abrasion-, and corrosion-resistant coatings for use in the pulp and paper, metals processing, and aluminum industries.

Experimental measurements are performed underrealistic processing conditions to obtain gas-phase concentrations, precursor decomposition kinetics, and deposition rates, using Sandia's high-temperature flow reactor (HTFR) equipped with a molecular-beam mass spectrometer. In addition, advanced characterization methods such as high-resolution transmission electron microscopy and energy-dispersion spectroscopy are used to characterize the microstructure and composition of reactor deposits. Computational tools developed through extensive research in the combustion field are employed to simulate the chemically reacting flows present in typical industrial reactors.

PROJECT TASKS

Two tasks for FY 1998 are defined as follows:

- **Task 1.** Chemical kinetics of precursor systems for float-glass coating
- **Task 2.** In situ process-control sensors for float-glass coating

The objective of Task 1 is to determine the thermodynamics and kinetics of chemical reactions occurring during the CVD of films on float glass, in particular those involved in the formation of indium tin oxide (ITO). Information obtained from this work is being used by CRADA partner Libbey-Owens-Ford (LOF) to develop new CVD processes at the pilot and manufacturing scales, using facilities available at LOF's research laboratories. Experimental measurements are performed underrealistic processing conditions to obtain gas-phase concentrations and precursor decomposition kinetics, using Sandia's HTFR. Computational quantum-chemistry tools also are being employed to (1) predict

thermochemical and kinetic data for gas-phase species present during the coating process and (2) simulate the chemically reacting flows present in typical industrial reactors.

The objective of Task 2 is to develop sensors for on-line control of float-glass coating processes. Information gained in Task 1 will be used to identify appropriate gas-phase species for detection, after which candidate sensor technologies will be identified and tested, both in laboratory reactors at Sandia and in pilot-scale reactors at LOF.

TECHNICAL PROGRESS: FY 1998

Summary

Efforts conducted this fiscal year were focused in two areas: (1) experimental and modeling investigations of the thermal stability and chemical reactions of CVD precursors used to deposit indium tin oxide (ITO) on float glass and (2) development of on-line sensors based on mass spectrometry for monitoring coating operations. The results of (1) show that organometallic compounds typically used to deposit ITO are sufficiently stable for extended periods of time to be stored at the elevated temperatures used to increase their vapor pressure. They also will survive transport through lengthy heated lines used to deliver them to coating reactors. Both experiments and modeling show that chemical bonds between indium and organic groups such as methyl are significantly stronger than previously reported in the literature, which accounts for this stability. However, we also learned that autocatalytic reactions on hot surfaces, such as those within the coating reactor, can accelerate dramatically the decomposition of compounds such as trimethylindium ($In(CH_3)_3$) and lead to nonvolatile products in these regions. Reactions with electron-donating additives such as hydrogen chloride also are very fast and may cause undesirable by-products to form that can lead to clogging of delivery and exhaust lines. In area (2), we performed laboratory tests of several potential methods for monitoring coating precursors and gas-phase products of the CVD reactions. Preliminary results indicate that mass spectrometry can be an effective on-line diagnostic, combining good sensitivity and the ability to distinguish between compounds of similar chemical nature with low cost and compact design. We constructed a prototype device that includes two sensors, one a standard residual gas analyzer, the other the Ferran Micropole™ analyzer, a novel device developed by NASA for achieving residual gas analysis in a small package. Both sensors will undergo field testing in FY 1999 at a float-glass facility owned by CRADA partner Libbey-Owens-Ford Co.

MILESTONES AND PROGRESS

Task 1: Chemical Kinetics of Precursor Systems for Float-Glass Coating

Thermochemistry and bond energies for CVD precursors used in glass-coating processes. Accurate thermodynamic data are an essential requirement for developing models of industrial coating processes. In the case of the materials typically used as coatings on float glass, these data, which consist of molecular heats of formation ($DH°_f$), heat capacities, and entropies, often are lacking. This is particularly true for indium-

containing precursors used to make indium tin oxide (ITO), such as trimethylindium [$In(CH_3)_3$; TMI]. Although the literature reports heats of formation for TMI (1) and $InCl_3$ (2), experimental data obtained in the HTFR (see below) indicate that the value for $In(CH_3)_3$ is incorrect. To obtain a better estimate for this value, we turned to quantum-chemistry methods (3), which have proven to be accurate to within ±2 kcal mol^{-1} in predicting heats of formation for main-group compounds for the first to third rows.

We performed a limited set of ab initio calculations on indium-containing compounds related to those used to deposit ITO. Calculations were performed at a relatively high level of theory (fourth-order Möller-Plesset perturbation theory using single, double, triple, and quadruple excitations), using the Stevens/Basch/Krauss/Jasien/Cundari-21G ECP Basis (SBKJC+ECP), which appears to be the best of the available (i.e., published) databases for indium. The accuracy of this basis set for predicting thermochemistry has not been tested, however. The results obtained are shown in Table 1.

Table 1. MP4(SDTQ) Predictions of Heats of Formation and Bond Energies for Indium-Containing Compounds

	$DH°_f$ (0 K), kcal mol^{-1}	
Compound	**Calculated**	**Literature**
InH_2CH_3	34.3	--
InH_2	68.7	--
$InCl_3$	–70.7	–87.9 ± 2.9[a]
$InCl_2$	–20.3	–47.7 ± 12[a]
CH_3	30.9	35.6 ± 0.2[b]
Cl	--	28.590 ± 0.001[b]

[a]See Ref. 2 below.
[b]See Ref. 4 below.

The results shown are not in particularly good agreement with reported literature values, in part due to the high uncertainty associated with these values and in part due to the known systematic errors in ab initio calculations stemming from basis-set truncation errors. However, they provide a rough indication that the In-C bond is considerably stronger than has been thought previously. Using the results in Table 1, we calculate an In-C bond energy in InH_2CH_3 of 65.3 kcal mol^{-1}. In contrast, the value obtained by Clark and Price (CP) from their flow-reactor experiments and typically cited by other investigators is 47.2 kcal mol^{-1}. We believe that our calculated In-C bond energy is likely to be an underestimate, based on experience in predicting bond energies for other main-group compounds. Unfortunately, even the In-Cl bond energy is not accurately known (an uncertainty of ±15 kcal mol^{-1} results from using the heats of formation reported by

Gurvich et al., shown in Table 1). Thus, we cannot be certain of the accuracy of the calculated value. Nevertheless, it seems likely that the value measured by CP is too low.

An alternative to direct calculations on indium-containing compounds is to examine trends in bond energies for compounds containing the lighter Group-III elements (i.e., B, Al, and Ga). These can be predicted by standard ab initio methods; in this case, we performed G2 calculations to predict the heat of formation. This high-level composite method is known to predict heats of formation for first- and second-row compounds to within 1 to 2 kcal mol^{-1} on average, and agreement with the limited data available for third-row compounds also is good. Bond energies calculated from the resulting heats of formation are shown in Table 2.

Table 2. Bond Energies in Group-III Compounds (kcal mol^{-1})

Species	M-C	M-Cl	M-OH
BCl_3		118.1	
$B(CH_3)_3$	103.9		
$AlCl_3$		117.8	
$AlCl_2(CH_3)$	86.1	121.9	
$AlCl(CH_3)_2$	84.5	124.9	
$Al(CH_3)_3$	84.2		
$Al(OH)_3$			130.3
$Al(OH)_2CH_3$			
$Al(OH)(CH_3)_2$			132.3
$GaCl_3$		100.4	
$GaCl_2(CH_3)$	76.2	105.7	
$GaCl(CH_3)_2$	75.8	112.2	
$Ga(CH_3)_3$	76.3		
$Ga(OH)_3$			79.0
$Ga(OH)_2CH_3$	78.5		76.6
$Ga(OH)(CH_3)_2$	77.6		73.6
$Ga(OH)(CH_3)Cl$	77.9	112.0	71.7
$Ga(OH)Cl_2$		104.6	69.0
$Ga(OH)_2Cl$		109.9	73.9

The results in Table 2 suggest several things about the bonding in Group-III compounds. First, M-C bonds (where M = B, Al, or Ga) decrease in strength as one proceeds from the first to the third row. For example, the bond energies for $M(CH_3)_3$ are 103.9, 84.2, and 76.3 kcal mol^{-1} for B, Al, and Ga, respectively. If this trend continues, one would expect the In-C bond in $In(CH_3)_3$ to be ≥68 kcal mol^{-1}. Again, this is considerably stronger than the value reported by CP (1). Second, M-C bonds essentially are unaffected by other substituents in the molecule, although M-Cl bonds decrease in strength with increasing numbers of Cl atoms bound to M. Third, M-OH bonds decrease in strength faster than $M\text{-}CH_3$ bonds as one goes from the first to the third row, to the point where they are comparable in Ga compounds. This suggests that there may not be a strong thermodynamic driving force to replace CH_3 with OH in indium compounds. Alternatively, there remains a substantial energetic advantage to replacing CH_3 with Cl. Thus, the reactions that occur in the gas phase likely are to involve HCl rather than H_2O or O_2, and the formation of In-O bonds may well occur only on the surface.

To summarize, our calculations suggest that In-C bond energies are substantially higher than those described in earlier literature reports. This confirms and supports our previous conclusion that, at least as far as gas-phase reactions are concerned, organoindium compounds should be sufficiently stable to be stored at moderately elevated temperatures and transported through heated lines.

Reaction kinetics of indium-containing precursors to ITO. Understanding of the thermal stability and chemical reactions (both gas-phase and surface) of CVD precursors is one of the most important aspects of developing a new coating process. The chemistry of the indium-containing precursors used to make ITO is in general quite poorly understood. Thus, a major part of our efforts in this project have been focused on improving the state of this knowledge. We used trimethylindium [$In(CH_3)_3$; TMI] for most of our experimental investigations because of its chemical similarity to other precursors of interest, ease of handling, and ready availability.

The objectives of this investigation were to (1) obtain experimental data to support theoretical estimates of the strength of the $In\text{-}CH_3$ bond, which is a direct indication of the thermal stability of compounds containing such bonds; (2) determine whether indium compounds containing methyl ligands are sufficiently stable to be stored for extended periods of time (as is the case under manufacturing conditions); (3) determine whether substantial degradation will occur during transport through long heated lines; and (4) measure the reaction rate with other compounds that may be present during the deposition process, such as HCl. All four objectives have been addressed; results are summarized below.

- Experimental data obtained from HTFR investigations indicate that, in all previously published studies of TMI decomposition (all of which involved flow reactors), TMI decomposition is dominated by processes occuring on hot reactor surfaces, rather than in the gas phase as previously was supposed. TMI undergoes an autocatalytic reaction that is preceded by a short induction period (e.g., $t < 7$ min at 673 K in Fig. 1). During the induction period, deposits form on the walls that apparently are quite reactive with

TMI and cause its decomposition to accelerate (e.g., Fig. 1, $t \bullet 7$ min at 673 K). Before these deposits form, however, TMI is stable in the gas phase at temperatures where it would be predicted to decompose completely, based on previously reported kinetic data (5). This behavior has not been previously documented and may be responsible not only for the large uncertainty associated with the measured values of the In-C bond energy, but also for the discrepancy between In-CH_3 bond energies derived from experimental data and those predicted by quantum theory. Results of this investigation were reported and published (see list of publications below).

- The combined HTFR data and theoretical results described earlier allow us to conclude that TMI and other chemically similar metallorganic precursors of interest for deposition of ITO should be stable under long-term storage conditions. It also should be possible to transport them through heated delivery lines without decomposition. This conclusion arises from the observation that the In-CH_3 bond strength in TMI is apparently significantly stronger than was thought by earlier investigators. Coupling the HTFR data with a theoretical analysis of the gas-phase decomposition of TMI by Buchan and Jaskinski (6) allows us to predict a lower limit for the bond energy of 58 kcal mol^{-1}, which is consistent with the ab initio predictions described above.

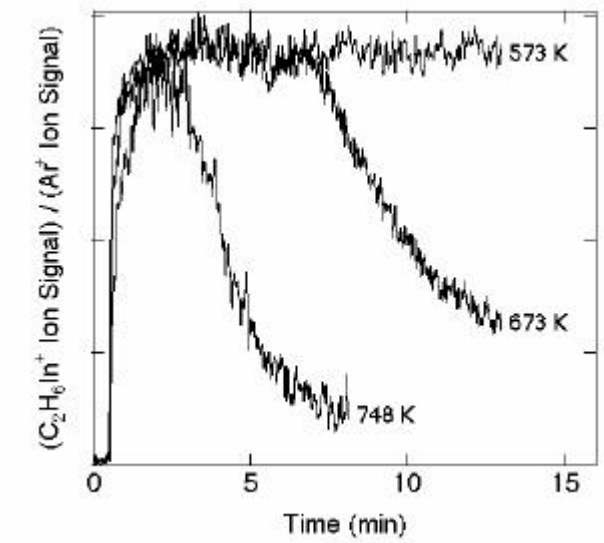

Fig. 1. Decay of the TMI mass-spectrometer signal as a function of time for different HTFR temperatures. Data were obtained at a fixed gas residence time at 10 torr for mixtures of 1000 ppm TMI in helium carrier gas.

- TMI reacts very rapidly with hydrogen chloride, an additive used by LOF in its process for making ITO films, to form dimethylindium chloride (DMIC) and methane:

$$In(CH_3)_3 + HCl \rightarrow (CH_3)_2InCl + CH_4 \quad (1)$$

This reaction goes to completion within 500 ms at temperatures as low as 348 K. Since DMIC is also a useful precursor for ITO formation, Reaction 1 can be an efficient method

for generating this compound in situ. Subsequent reaction of DMIC with HCl appears to be significantly slower, suggesting that formation of less volatile higher chlorides (which could condense and clog delivery lines or narrow spaces within a reactor) should not be a problem.

Improvements to experimental facilities. Characterization of the chemical processes occuring during CVD coating of float glass involves many experimental complexities that we have not encountered in precursor systems we previously investigated. These include extensive fragmentation of parent molecules in the mass spectrometer, which complicates data interpretation; high surface reactivities; and low precursor vapor pressures. To mitigate some of these effects and facilitate investigation, we upgraded several systems associated with the HTFR:

- A high-frequency modulator (800 Hz) was installed in the molecular-beam mass-spectrometer system to increase the phase-angle resolution of this instrument, substantially improving our ability to associate ion fragments formed in the spectrometer with their correct parent molecule. This is extremely important for understanding the chemistry of many coating systems because the ion fragments of reactants and products often have the same molecular weight.
- A test cell equipped with an FTIR spectrometer and a residual gas analyzer (RGA) was constructed (Fig. 2). This system allows for rapid, qualitative characterization of CVD precursor chemistry and has assisted us in the evaluation and development of potential diagnostic systems that could be used for on-line process monitoring.

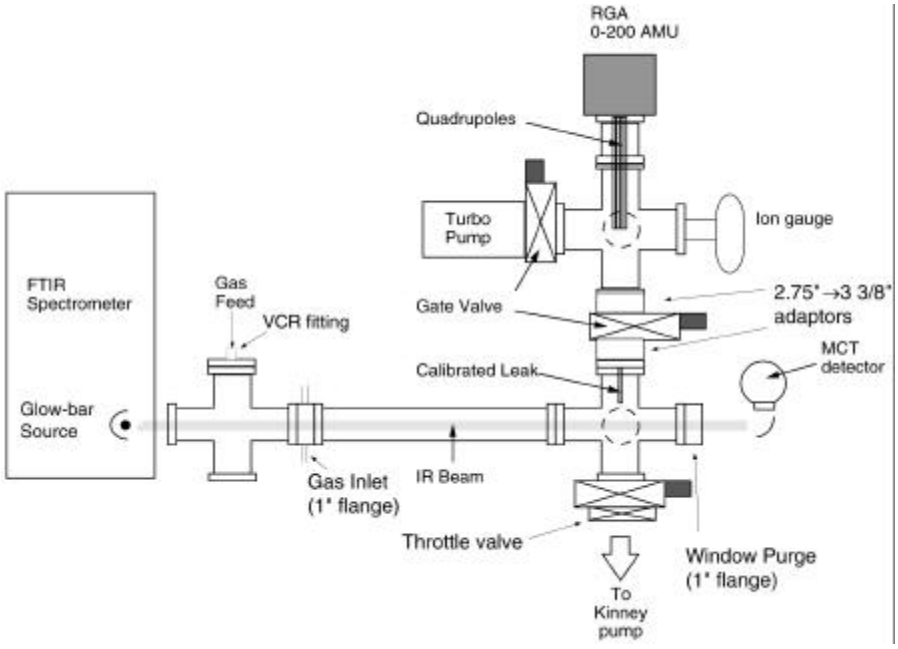

Fig. 2. Laboratory test cell for evaluating potential process-monitoring technologies.

Interactive Web site for thermochemical and kinetic data under construction. This project and previous investments by the AIM Program have yielded a wealth of

information of thermodynamic and kinetic data that could find application to a range of industrial materials processes. In order to provide the greatest possible access to the information generated by this project, we constructed an interactive web site that can be found at the following URL:

http://www.ca.sandia.gov/CRF/Research/Applied/ThermoKinData/

Two types of data are available: (1) thermodynamic properties (heats of formation, entropies, and heat capacities) for gas-phase molecules relevant to CVD and other high-temperature processes and (2) kinetic mechanisms that describe gas-phase and/or surface chemical reactions occurring during CVD process. Although construction of a Web site is not one of the tasks envisioned in the original project plan, the explosive growth of the Internet in the last 2 years has demonstrated that this can be a very effective tool for communication and dissemination of information.

The site allows the user to scan a list of molecules and reaction mechanisms, choose those of interest, and then download to a personal computer the corresponding thermodynamic and kinetic data in Mac, PC, or Unix formats. Thermodynamic data are available as polynomial fits in the format originally defined by NASA and later adopted for Sandia's CHEMKIN (7) Thermodynamic Data Base. The CHEMKIN suite of subroutines is widely used by both industry and academia to analyze CVD, combustion, and other high-temperature processes, and thus provides a convenient way for users to apply our data to their own problems. We also provide extensive comments and references so that the user is aware of the source of the data and will know where to look for additional information. Thermodynamic data for the following chemical systems are currently available:

- B-N-H-Cl compounds (33 species)
- Si-C-H compounds (34 species)
- Si-C-Cl-H compounds (49 species)
- Si-O-H compounds (47 species)
- $TiCl_x$ compounds; x = 1 – 4
- Si-boron
- Aluminum compounds

Task 2: In Situ Process-Control Sensors for Float-Glass Coating

Several advances were made this year toward the development of an on-line monitor of process gases during the deposition of coatings on float glass. The ultimate goal of the process monitor is to identify key chemical signatures in either the supply or exhaust lines that would directly relate to product quality and that correspond to macroscopic changes in such process conditions as feed composition, exhaust-gas flow rate, and substrate temperature.

Evaluation of diagnostic methods: FTIR and mass spectrometry. Two techniques with the potential to serve as an on-line process monitor were evaluated: Fourier-transform infrared spectrometry (FTIR) and mass spectrometry (MS). Experiments were performed in a heated test cell (Fig. 2) through which coating precursors and carrier gases flowed under conditions that simulated the gas composition, temperature, and pressure of the Libbey-Owens-Ford (LOF) chemical supply lines. Two different ITO precursors were used: TMI and DMIC. The purpose of these experiments was to evaluate the sensitivity of the two techniques and to look for potential measurement interferences (such as overlap between spectral features of different molecules). As will be seen from the following discussion, MS emerged as the most promising technique. We will briefly discuss the results of the tests of FTIR as well, however.

The FTIR results confirmed the presence of both TMI and DMIC, as well as the emergence of vibrational features indicative of the expected product gases. These results are in complete agreement with earlier experiments performed in the HTFR using mass-sampling techniques and serve as an independent verification of our proposed method for generating DMIC in situ (see above). A second set of experiments was then conducted in order to search for any unique infrared spectral features belonging to these compounds that could be used to develop an on-line process monitor. We found that DMIC and TMI exhibit strong vibrational bands that can be used to monitor their concentrations in a reacting-flow environment. However, because of the similarity of these two precursors to indium-containing by-products that might form, coupled with an inability to collect spectra at wave numbers shorter than 600 cm^{-1} where In-Cl stretching frequencies are expected to be found (a limitation of our FTIR spectrometer), we could not identify a unique signature from which to distinguish DMIC from TMI. An additional problem associated with FTIR is the requirement for optical access, which can be difficult to achieve in a manufacturing environment. We thus conclude that FTIR would be difficult to implement as an on-line monitor of the ITO CVD process.

We next evaluated the performance of a Ferran Micropole™ analyzer (MPA) in the categories of sensitivity and mass resolution. The MPA is a novel device developed by NASA for achieving residual gas analysis in a small package that is less demanding, in terms of space and ownership costs, than conventional RGA instruments. In so doing, the MPA trades size and cost for resolution and sensitivity. In experiments performed this quarter, the signal response of an MPA was benchmarked against that of a Leybold Inficon Transpector™ (LIT), which is a precision RGA capable of collecting high-resolution mass spectra from 0 to 300 amu, for 6 gas-phase moieties specific to the LOF coating process.

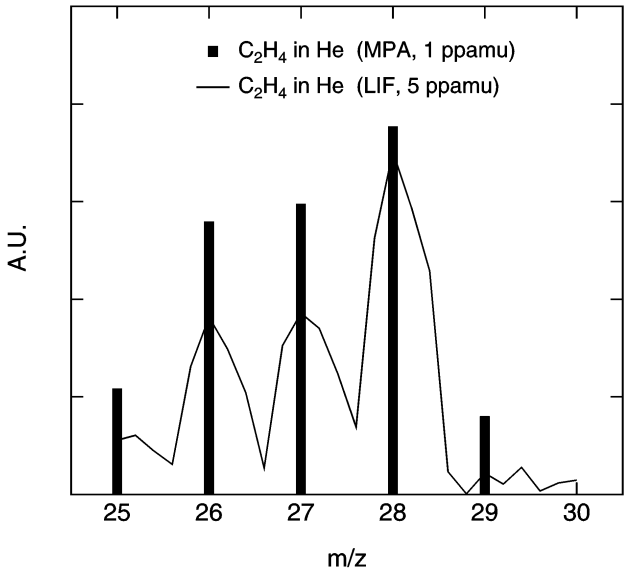

Fig. 3. Signal intensity as a function of m/z for C_2H_4 in He carrier gas. Comparison between the mass resolution of the LIF (solid line at 5 points per amu) and the MPA (solid bar at 1 point per amu). The MPA is at maximum resolution.

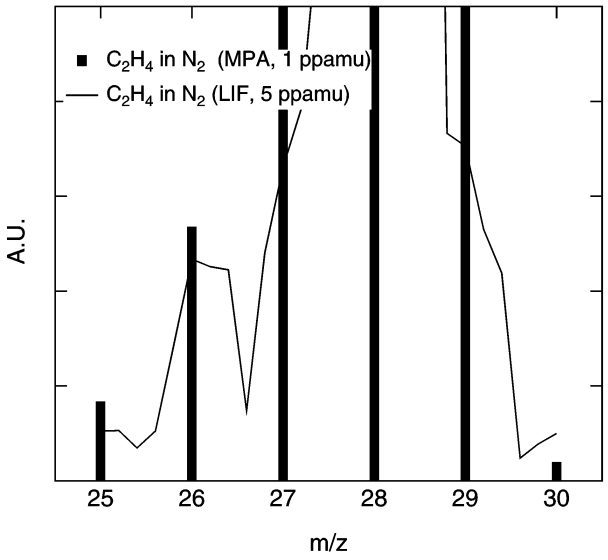

Fig. 4. Signal intensity as a function of m/z for C_2H_4 in N_2 carrier gas. Comparison between the mass resolution of the LIF and the MPA. Here the large m/z 28 peak of N_2 appears to obscure the C_2H_4 signature.

We will illustrate the performance of the MPA with results obtained for the detection of C_2H_4, which is a reactant used in the formation of tin oxide films. All experiments were performed in the test cell at atmospheric pressure, 473 K, in either pure He or N_2 ambient. The experimental results are illustrated in Figs. 3–6. It is clear from the data presented in these figures that, while the MPA lacks the mass resolution of the LIT, it has sufficient resolution and sensitivity to successfully monitor the C_2H_4 concentration even in the presence of a large N_2 background. This fact remains true for five other low-molecular-weight gases (<100 amu) involved in the deposition process.

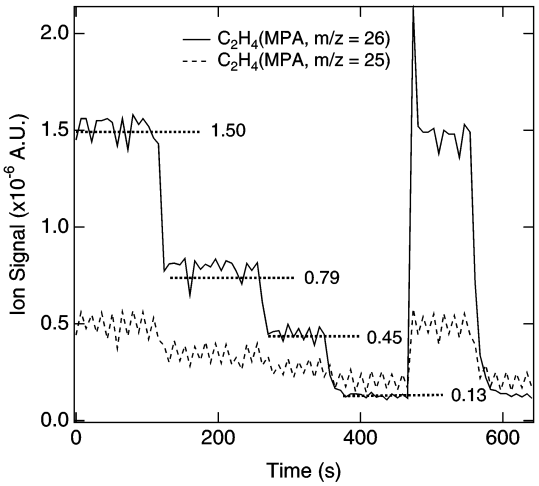

Fig. 5. MPA signal at m/z 25 and 26 as a function of experiment time. Each plateau in the signal represents a different flow rate of C_2H_4 into the cell. The large N_2 signal in Fig. 5 obscures m/z 27 and 28 but not m/z 25 and 26.

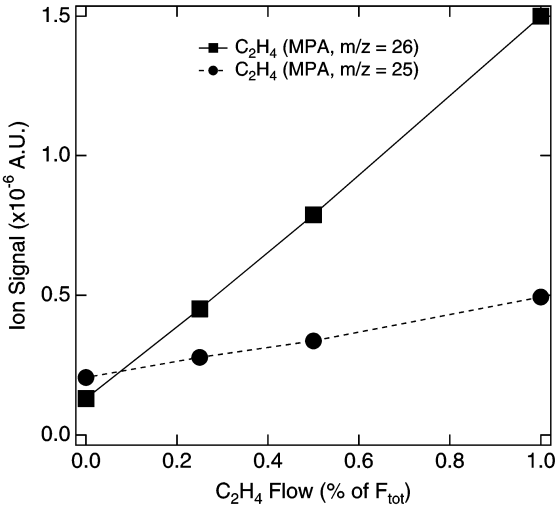

Fig. 6. Average MPA signals at m/z 25 and 26 as a function of % by volume of total flow for C_2H_4 in test cell. A linear response is observed for both peaks, with an ultimate detection limit of less than 0.1% for the m/z 26 peak.

The results of the experiments with the MS systems give us confidence that an RGA system such as the MPA can be used for process monitoring of the supply lines to float-glass coating reactors. However, an RGA may not provide the desired information for the chemical composition of the exhaust-gas mixture, since deposition reactions likely will produce species in the m/z 15 to 50 range that may obscure the desired chemical signatures. To test this hypothesis, we have assembled a detailed kinetic model to predict the identities and relative concentrations of the most significant compounds expected to be produced during the deposition process for tin oxide (see section below, "Silane Oxidation"). However, a true test of the system's performance can be verified only by on-site testing in a float-line coating facility. To this end we have constructed a mass-sensing unit (see below) that will be tested at LOF's Ottowa, Illinois, facility in early FY 1999.

Field-Portable Sensor. The gas-sampling manifold used in the experiments described thus far has undergone substantial modifications in order to produce a field-portable unit for in-house testing at the LOF float-glass facility in Ottawa, Illinois. Following detailed discussions with LOF personnel, we designed and assembled a transportable vacuum

manifold that is able to withstand the rigors of plant operation. It also is desirable to be able to sample multiple gas streams with the same sensor in order to compare and contrast the constituents of each stream in real time. This capability was not incorporated into the original design but has since been realized. Pictured in Fig. 7 is a gray-scale image of the new field-portable RGA system.

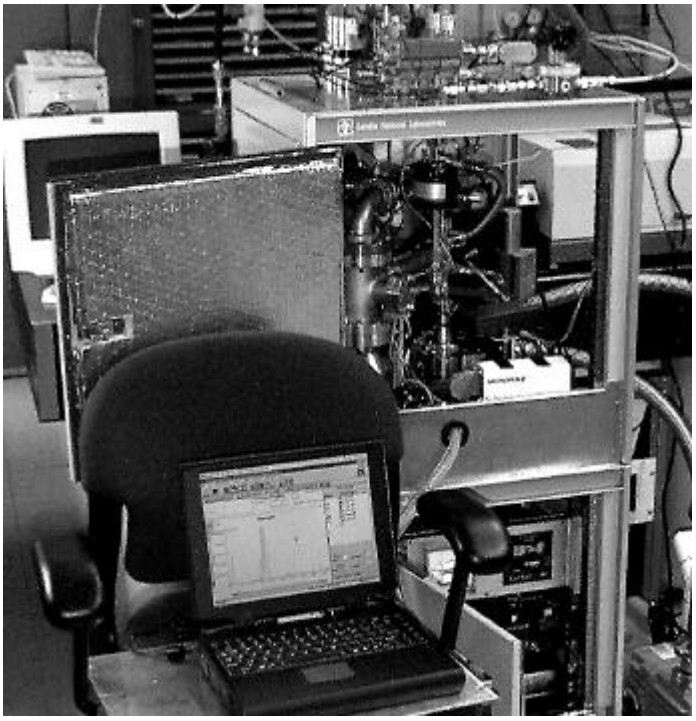

Fig. 7. Photograph of field-portable RGA system.

Figure 8 presents a schematic of the system showing a low-vacuum, pressure-regulated valving manifold (Stage 1) coupled to a high-vacuum chamber (Stage 2) via a precision leak-valve. The Stage 2 chamber houses the LIT and MPA gas analyzers as well as a turbo-molecular pump and cold cathode gage. It operates at pressures between 10^{-8} to 10^{-4} torr. Stage 1 has two sample lines (Line 1 and Line 2 in Fig. 8) that interface directly into the LOF process streams. Each sample line is terminated with a 250-μm orifice that chokes the gas flow and thereby establishes the ultimate throughput into the probe. The remainder of Stage 1 is composed of a pneumatically operated switching manifold (valves labeled A and B in Fig. 8) that diverts flow from *either* sample line to the precision leak-valve, and a control loop for maintaining the operating pressure of Stage 1 in the range of 5 to 10 torr. The field unit is remotely operated via a laptop computer and is capable of collecting data at rates much faster than 1 Hz. The time required for the system to respond to process changes is determined ultimately by the length of tubing that connects the sample lines to the process. Conservative estimates place system dead time around 5 to 15 s.

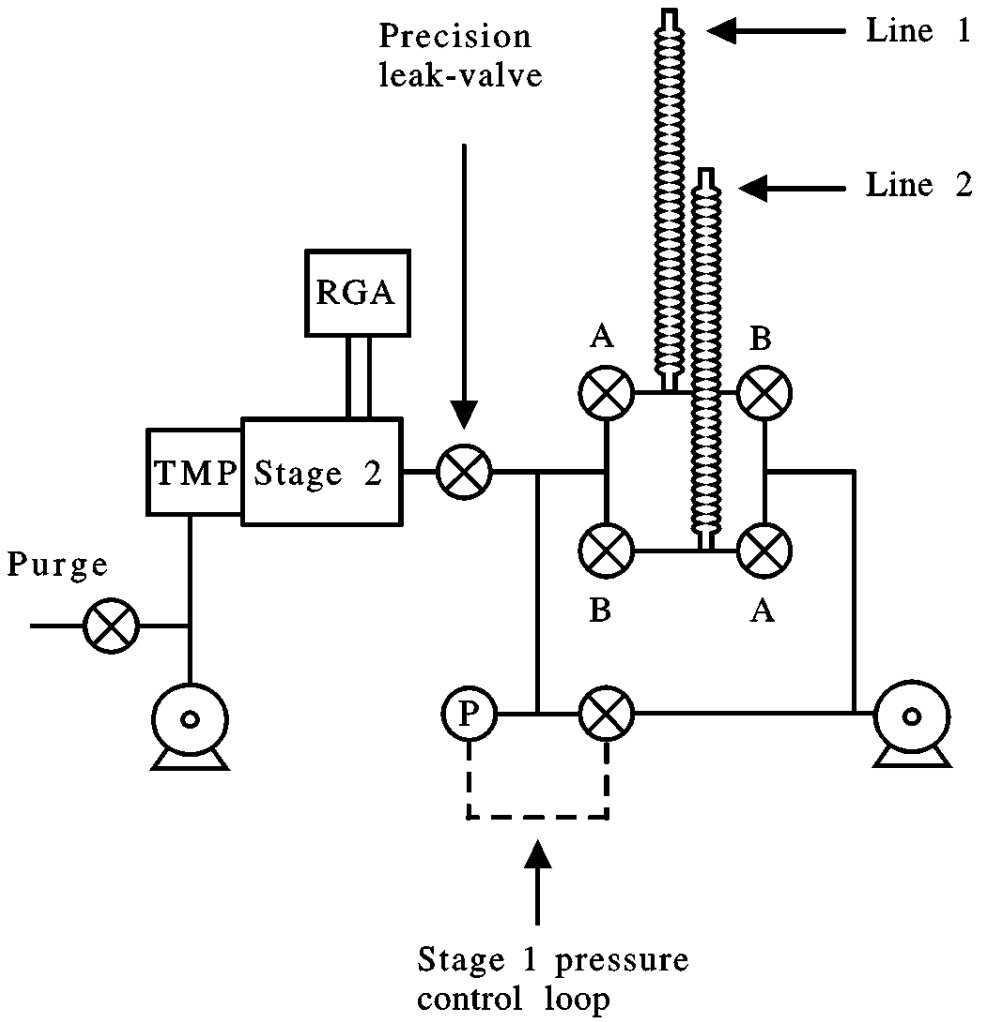

Fig. 8. Schematic of field-portable RGA system.

Silane Oxidation. As mentioned earlier, the full utility of the RGA probe may be difficult to realize if the CVD reaction produce gases with spectral features that overlap the more important mass signatures relating to product quality. In an effort to evaluate the likelihood of potential problems, we formulated a kinetic model of silane oxidation that closely resembles the LOF silica-deposition process. The reaction mechanism is quite comprehensive and contains 376 reactions between 65 gas-phase species. Currently, we are using SENKIN to integrate the rate equations over a specified temperature profile, neglecting hydrodynamic and transport effects. The simulations identified a few oxygenated hydrocarbon products present at concentrations high enough to interfere with the interpretation of the mass spectra in the critical mass range of m/z 15 to 50. Knowing that these potential problems exist beforehand undoubtedly will aid in the successful implantation of our process monitor.

REFERENCES

1. W. D. Clark and S. J. W. Price, *Can. J. Chem.* **46,** 1634 (1968).
2. L. V. Gurvich, I. V. Veyts, and C. B. Alcock, *Thermodynamic Properties of Individual Substances,* CRC Press, Boca Raton, 1994.
3. C. F. Melius, M. D. Allendorf, and M. E. Colvin, in *Fourteenth Intl. Conf. on Chem. Vapor Dep./EUROCVD-11*, The Electrochemical Society, Pennington, 1997, p. 1.
4. M. W. Chase, C. A. Davies, J. R. Downey, D. J. Frurip, R. A. McDonald, and N. A. Szverud, *J. Phys. Chem. Ref. Data* **14**, (1985).
5. M. G. Jacko and S. J. Price, *Can. J. Chem*. **42,** 1198 (1964).
6. N. I. Buchan and J. M. Jasinski, *Cryst. Growth* **106,** 227 (1990).
7. M. E. Coltrin, R. J., Kee, F. M. Rupley, E. Meeks, and J. A. Miller, "Chemkin-III: A Fortran Chemical Kinetics Package for the Analysis of Gas-Phase Chemical and Plasma Kinetics" and "Surface Chemkin-III: A Fortran Package for Analyzing Heterogeneous Chemical Kinetics at a Solid-Surface–Gas-Phase Interface," Sandia National Laboratories SAND96-8216-UC-405 and SAND96-8217 UC-406, 1996.

PUBLICATIONS AND PRESENTATIONS

Reviewed Journal Articles and Proceedings Papers

C. W. Bauschlicher, Jr., C. F. Melius, and M. D. Allendorf, "Gallium compounds, A Possible Problem for the G2 Approaches," accepted for publication in *J. Chem. Phys.*, 1998.

M. D. Allendorf and C. F. Melius, "Understanding Gas-Phase Reactions in the Thermal CVD of Hard Coatings Using Computational Methods," accepted for publication in *Surf. Coatings Technol.*, 1998.

A. H. McDaniel and M. D. Allendorf, "A Flow-Tube Investigation of the High-Temperature Reaction Between BCl_3 and NH_3," *J. Phys. Chem.* **102**, 7804 (1998).

F. Teyssandier and M. D. Allendorf, "Thermodynamics and Kinetics of Gas-Phase Reactions in the Ti-Cl-H System," *J. Electrochem. Soc.* **145**, 2167 (1998).

M. D. Allendorf and A. H. McDaniel, "Kinetics of Reactions Relevant to the Chemical Vapor Deposition of Indium Compounds," *Chemical Aspects of Electronic Ceramics Processing*, Materials Research Society, vol. 495, p. 125, 1997.

PRESENTATIONS

A. H. McDaniel and M. D. Allendorf, "Flow-Tube Measurements of the Rate Constant for the Gas-Phase Reaction Between Boron Trichloride and Ammonia," AIChE Meeting, November 1997.

M. D. Allendorf and A. H. McDaniel, "Kinetics of Gas-Phase Reactions Relevant to the Chemical Vapor Deposition of Indium Compounds," *Chemical Aspects of Electronic Ceramics Processing*, Materials Research Society Fall Meeting, Boston, 1997.

M. D. Allendorf, "Gas-Phase Thermochemistry and Kinetics Relevant to the CVD of Ceramic Coatings: New Data for Process Models," invited paper presented at the Intl. Conf. Metallurgical Coatings and Thin Films, San Diego, April 1998.

M. D. Allendorf, S. Ferko, A. McDaniel, and C. F. Melius, "Thermochemistry and Kinetics for CVD Modeling: Good News and Bad News," invited lecture presented at the Gordon Conference on High-Temperature Chemistry, July 21, 1998.

HONORS AND AWARDS

M. Allendorf presented two invited lectures (Nos. 3 and 4 above).

PATENTS/DISCLOSURES

None.

LICENSES

None.

INDUSTRIAL INPUT AND TECHNOLOGY TRANSFER

LOF continued to share their data concerning the CVD of coatings on float glass with Sandia efforts to understand the chemical reactions in these processes and to develop new sensors for process control.

COST SHARING

LOF provided $180K of direct and in-kind cost sharing to support investigations of float-glass coating chemistry.

ESTIMATED ENERGY SAVINGS

In North America, 2.6 million tons/year of float glass are used in residential and commercial construction. Use of so-called "low-E" (for "low-emissivity") coatings on this glass can improve dramatically the energy efficiency of this material. New coatings developed in this project will save 1.4×10^{13} Btu/year when installed in place of clear glass windows.

High Temperature Particle Filtration Technology

T. M. Besmann and R. L. Martin
Metals and Ceramics Division
Oak Ridge National Laboratory
P.O. Box 2008, Oak Ridge, Tennessee 37831

C. A. Hall
Dow Corning Corp.
4770 Highway 42 East
Carrollton, Kentucky 41008

INTRODUCTION

THe Dow Corning Corporation is a market leader in the production of dimethyldichlorosilane (DDS), which is used as an intermediate in a wide variety of silicone products. In Carrollton, Kentucky, Dow Corning currently operates the largest plant of its type for the production of DDS, housing several generations of production streams. The facility could benefit substantially, both in process-stream efficiency and effluent cleanup, from improved high-temperature filtration technology. The technical objective of the CRADA with Dow Corning was to assess the usability of high-temperature filtration materials and technology for application in processes to produce DDS and for effluent cleanup for chlorosilane and chemical-grade silicon production. A bench-scale furnace and gas-flow system were designed and built to simulate two particular processing environments. The first environment, called the fluidized bed reactor (FBR) environment, ran at 290°C with gas-flow rates of 500 cc/min of methyl chloride and 2.7 ml/min of DDS. The second environment, called the thermal oxidizer (THROX) environment, ran at 1040°C with gas-flow rates of 9.6 cc/min of hydrogen chloride and 887 cc/min of mixed gas consisting of nitrogen, oxygen, carbon dioxide, and water vapor. Filter specimens were collected from various manufacturers and exposed to simulated process environments for different times. The filter media included carbon, silicon carbide, oxide ceramics, and metal alloys. All of the samples were in the form of rings 2.5 cm in height, obtained from candle filter shapes. After exposure, the specimens were characterized, and mechanical-properties testing was carried out to determine the feasibility of using the various types of filter materials. Three unexposed samples of each material also were characterized. The strength test consisted of filling the volume of the ring with elastomer and then bursting the sample by applying pressure to the elastomer with a plunger in test frame. Displacement was measured via sensors on the circumference of the ring, and burst pressure was recorded.

TECHNICAL PROGRESS: FY 1998

All rings slated for FBR testing were exposed for 24 h and rupture tested to assess the mechanical strength. The rupture data were compiled and presented to Dow Corning staff via a televideoconference on November 12, 1997. Both the as-received and after-exposure

mechanical-strength properties of each filter ring type were discussed in an effort to down-select samples for the next test series. Several material types were eliminated for various reasons. We collectively decided to pursue seven material types for the 1000-h FBR exposure. Before the 1000-h test, however, we ran FBR simulations for 72 h with the filters in direct contact with captured silicon powder from the Dow Corning manufacturing plant. Burst testing on these particular samples demonstrated that no loss in mechanical strength occurred due to the exposure to the furnace conditions and contact with the powder. After several furnace modifications to interlock some safety features and after modifying the system to recycle the DDS from the exhaust end back to the source cylinder, we proceeded with the 1000-h FBR testing. A sample of the recycled DDS was sent to the Dow Corning plant for analysis to ensure that no changes were taking place chemically. This analysis assured us that the DDS underwent no changes during the long 1000-h runs. Surprisingly, no significant mechanical-strength losses occurred after the 1000-h furnace exposure. Apparently all materials to which we down-selected were promising candidates. A summary of the filter test results is presented in Table 1.

A scrubber was designed and built as an addition to the bench-scale system to treat the exhaust gases during the THROX simulation runs. After these furnace modifications, we commenced 24-h THROX simulations. All material types slated for THROX conditions were tested. Rupture testing on these materials demonstrated no significant loss of mechanical strength due to exposure.

Table 1. Summary of Filter Specimen Test Results

Manufacturer	Type	Control		FBR		Therm. Ox.
			24 h	72 h	1000 h	24h
		(MPa)	(MPa)	(MPa)	(MPa)	(MPa)
Dupont-Lanxide	SiC/SiC	37.36	41.39	45.85	31.55	30.64
Dupont-Lanxide	PRD-66C	6.75	6.6	7.86	6.12	6.37
Dupont-Lanxide	PRD-66M	4.72	5.41	6.42	6.67	5.7
3M Company	SiC/Nextel	11.34	9.64	13.14	10.65	Incomplete
Techniweave	Carbon/SIC	11.4	11.34	11.41	12.23	FBR Only
Techniweave	Mullite/Mextel 610	22.19	Thermal Oxidizer Only			22.37
Techniweave	Mullite/Nextel 720	14.69	Thermal Oxidizer Only			13.57
Smart Ceramics	Oxide	28.59	32.69	26.37	24.84	29.23
McDermott Technologies	Oxide	8.94	9.11	-	8.87	8.32
Amercom	SiC	1.15	0.56	**		
Amercom	Oxide	0.75	0.64	**		
Blasch	Oxide	4.62	4.65	**		
Pall Corporation	Hastelloy X	205.71	256.86	260.85	208.4	FBR Only
Pall Corporation	Hastelloy C276	65.6	60.37	*		FBR Only
Pall Corporation	Inconnel 600	144.35	148.21	*		FBR Only
Pall Corporation	Vitripore 326	15.57	Thermal Oxidizer Only			14.48
*Dropped since not commercially available						
**Eliminated by properties						

MEETINGS

T. M. Besmann and M. A. Karnitz of ORNL and Merrill Smith, the Department of Energy CFCC Program Manager, attended a meeting held at the Dow Corning plant in Carrollton, Kentucky, on September 3, 1998, to discuss results.

PRESENTATIONS

T. M. Besmann, "High Temperature Particle Filtration," Advanced Industrial Materials Program Annual Meeting, 1998, Jackson Hole, Wyoming, June 23–25, 1998.

D. J. Bennett, "Hot Gas Filters," NACE International, Ceramics: Cutting Edge Solutions for Corrosion Control, Houston, Texas, June 29–30, 1998.

Membrane Systems for Energy-Efficient Separation of Light Gases

D. J. Devlin, T. Archuleta, and R. Barbero
Los Alamos National Laboratory
MS E549, MST-7
P.O. Box 1163
Los Alamos New Mexico 87545

M. Carrera
Amoco Research Center
P.O Box 3011
Naperville, Illinois 60566-7011

INTRODUCTION

Ethylene and propylene are two of the largest commodity chemicals in the United States, and they are major building blocks for the petrochemicals industry. These olefins are separated currently by cryogenic distillation, which demands extremely low temperatures and high pressures. Over 75 billion pounds of ethylene and propylene are distilled annually in the United States at an estimated energy requirement of 400 trillion Btu. Nondomestic olefin producers are rapidly constructing state-of-the-art plants. These energy-efficient plants are competing with an aging U.S. olefins industry in which 75% of the olefins producers are practicing technology that is more than 20 years old. New separation opportunities, therefore, are needed to continually reduce energy consumption and remain competitive. Amoco has been a leader in incorporating new separation technology into its olefins facilities and has been aggressively pursuing noncryogenic alternatives to light-gas separations. The largest area for energy reduction is the cryogenic isolation of the product hydrocarbons from the reaction by-products, methane and hydrogen. This separation requires temperatures as low as -150^{o}F and pressures exceeding 450 psig. This CRADA will focus on developing a capillary condensation process to separate olefinic mixtures from light-gas by-products at temperatures that approach ambient conditions and at pressures less than 250 psig; this technology breakthrough will result in substantial energy savings. The key technical hurdle in the development of this novel separation concept is the precise control of the pore structure of membrane materials. These materials must contain specially shaped channels in the 20- to 40-Å range to provide the driving force necessary to remove the condensed hydrocarbon products. In this project, Amoco is the technology end-user and provides the commercialization opportunity and engineering support. LANL provides the material-development expertise that is critical for achieving the desired product separation.

TECHNICAL PROGRESS: FY 1997

Summary

The development of thin films with controlled pore size in the nanometer range is an objective of this program. The separations approach is based on the capillary condensation of hydrocarbons in 1- to 5-nm pores. Figure 1 illustrates one version of the concept.

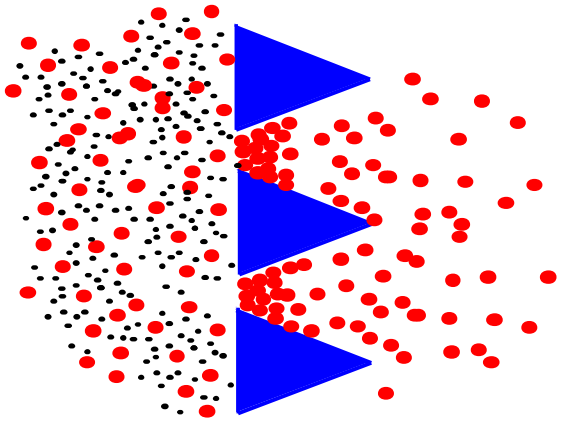

Fig. 1. Illustration of capillary condensation of hydrocarbons in a porous substrate.

In this approach, a feed consisting of hydrocarbon and hydrogen gas pass over the up-stream side of the membrane. Preferential condensation of the hydrocarbon in the pores occurs, blocking them with hydrocarbon and restricting flow of hydrogen. The hydrocarbon is transported through tapered pores and evaporated on the large-pore diameter side, leaving a hydrogen-rich feed. The actual operating conditions will depend on the pore size, geometry, and membrane permeability.

Thin-film deposition by evaporation and sputter techniques can result in porous microstructures. These microstructures typically consist of columnar grains separated by porous regions. The development of porous structures is dependent on a number of such deposition parameters as substrate temperature, deposition rate, ambient atmosphere, angle of incidence, and energy of depositing flux. Porous structures generally are observed for conditions where the surface mobility of depositing atoms is limited. The direction of columnar growth is related to the angle of incidence according to the relationship known as the tangent rule:

$$\tan(\beta)=1/2\ \tan(\alpha) \qquad (1)$$

where α is the angle between the surface normal and the direction of the vapor flux and β is the angle between the surface normal and growth direction, Fig. 2. While this exact relation does not always hold, it is universally found that the angle β is less then α. The effect is a consequence of a process known as “self shadowing” (1–3). This occurs when deposited atoms exposed to the incoming vapor flux shield the substrate or unoccupied

sites from direct impingement. When the surface mobility is low, so that rearrangement to fill the shielded sites is not possible, columnar grains form.

The dimensions of the pore in simplistic terms are dependent on the incident angle and size of the shadowing adatom, cluster, or nuclei. Crystallographic effects also can be important in defining the grain structure. Substrate temperature and therefore mobility will effect nuclei size and rearrangement. Also, the energy and distribution of the atomic flux and degree of thermalization of the beam are important. For carbon materials sputter-deposited at room temperature, the surface mobility is low. A comparison of the TEM micrograph of an oblique-angle–evaporated film to a simulation under similar experimental conditions is shown in Fig. 3.

The simulation predicts the correct angle of the growth of the carbon grains. Furthermore, it is in reasonable agreement with the pore size and grain size observed in the TEM.

Membrane Fabrication

The fine-pore side of an alumina Anodisc™ filter provides a suitable substrate for the deposition of carbon films with a 4- to 5-nm pore dimension. Films were deposited with a 10-cm–diam, RF-powered magnetron sputter gun in a high-vacuum system. The arrangement is illustrated in Fig. 4.

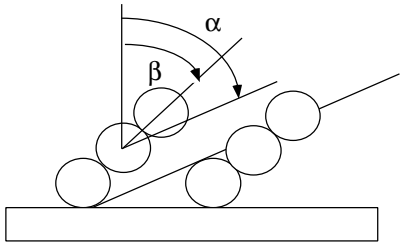

Fig. 2. Self shadowing of vapor flux during oblique angle deposition. a **is the angle of the incoming beam,and** b **is the direction of columnar grain growth.**

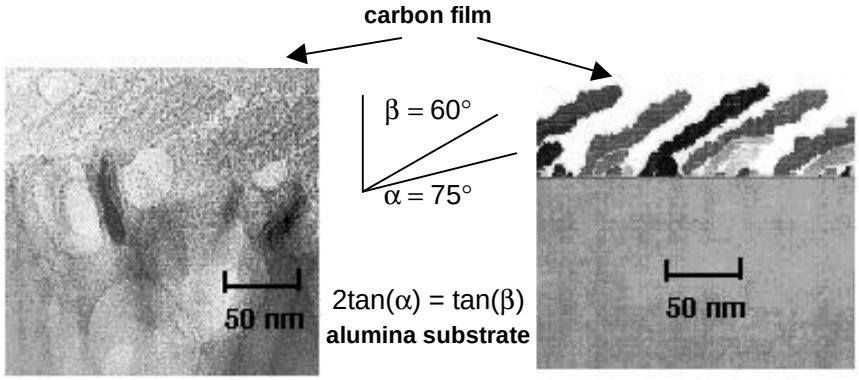

Fig. 3. Comparison of thin film deposition process simulation to TEM micrograph of evaporated carbon film.

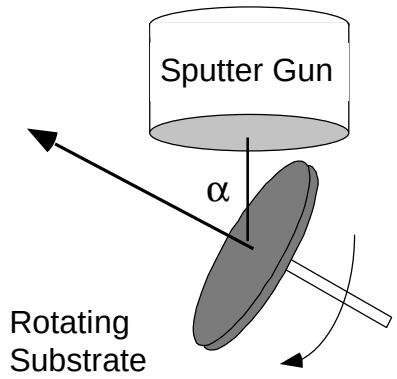

Fig. 4. Illustration of the oblique-angle deposition arrangement used in this study.

Substrates were set at an angle with respect to the gun and rotated. The angle can be continuously varied to provide a tapered pore structure. Rotation of the stage improved uniformity and altered the microstructure. Typical sputter conditions were argon pressures of 0.1 to 0.3 Pa and RF power of 90 watts. Deposition rates were on the order of 100 nm/h, and angle of incidence varied from 0º to 85º. Figure 5 shows a typical microstructure produced by this deposition technique. Pores are on the order of 5 nm as discussed in more detail in previous reports (4).

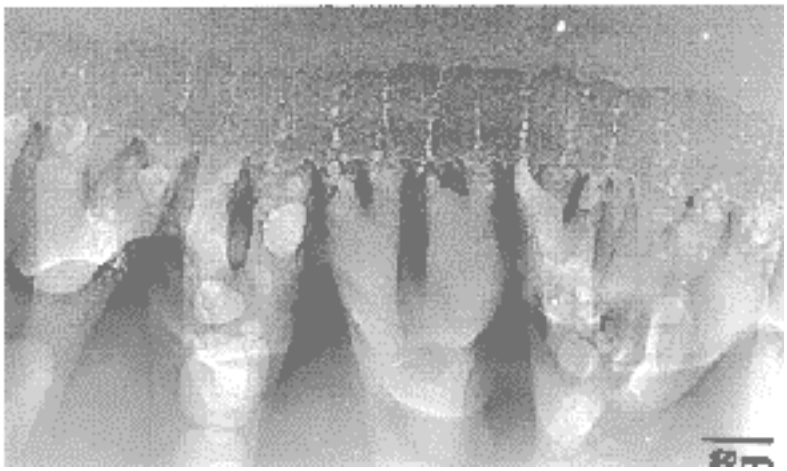

Fig. 5. TEM micrograph showing the effect of rotating the substrate during deposition.

DISCUSSION

The separation of gaseous components by capillary condensation depends on both thermodynamic and kinetic effects. For gas mixtures condensed in pore space, the condensed-liquid phase is enriched in the heavy, more condensable components. This is illustrated in Fig. 6 for an ideal binary solution. The curve labeled r represents the

liquid/vapor equilibrium for the small-pore side and r´ represents the large-pore equilibrium curve. At some point a radius will be reached where the liquid composition will evaporate congruently at P´, resulting in vapor-phase composition, Y´ = X

In practice, however, in order to maintain a stable meniscus, large pressure drops on the order of several hundred psi are necessary. This is not desirable for a large-scale operation due to the associated costs of compressors and/or vacuum equipment. If we operate with no pressure drop and transport through the membrane is rapid, so that equipment vapor pressures are achieved, then no separation is expected to occur. That is, evaporation on the down-stream side should result in the same gas composition as that on the up-stream side. This is not what we observe. Separation factors tend to be close to that predicted on the basis of the condensed-liquid composition. Figure 7 shows the result of calculated separation factors relative to methane based on the estimated condensed-liquid compositions. Similar results were obtained for actual gas mixtures tested.

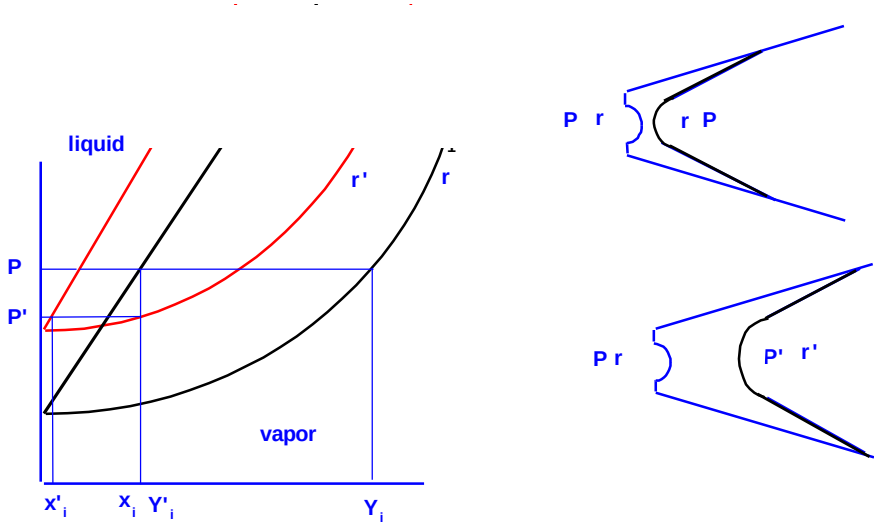

Fig. 6. Illustration of the use of tapered pores in a separation process by capillary condensation of an ideal binary solution.

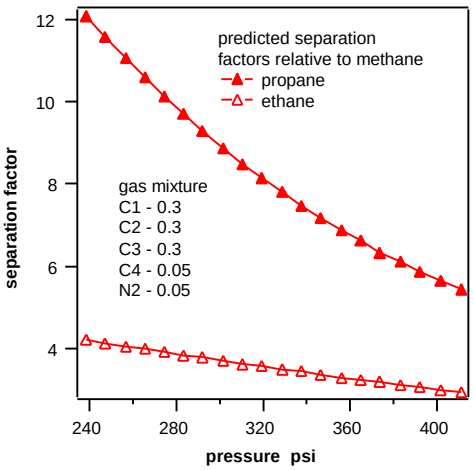

Fig. 7. The results of calculated separation factors relative to methane based on the estimated condensed liquid compositions for a gas mixture of nitrogen, methane, ethane, propane, and butane. Calculations performed on ASPEN process simulator.

Similarly, the system of propylene and hydrogen showed separation factors ranging from 300 to 5000 (see Fig. 8). The upper end of these values is clearly consistent with the estimated mole fraction of hydrogen in the condensate, x = 0.0004. Under the conditions in which our permeation cells are operated, equilibrium vapor pressures are not achieved downstream. The estimated evaporation rates suggest that transport through the membrane limits the flux. Thus, pore blockage combined with relatively slow diffusion of hydrogen through the liquid hydrocarbon is responsible for the high separation factors observed.

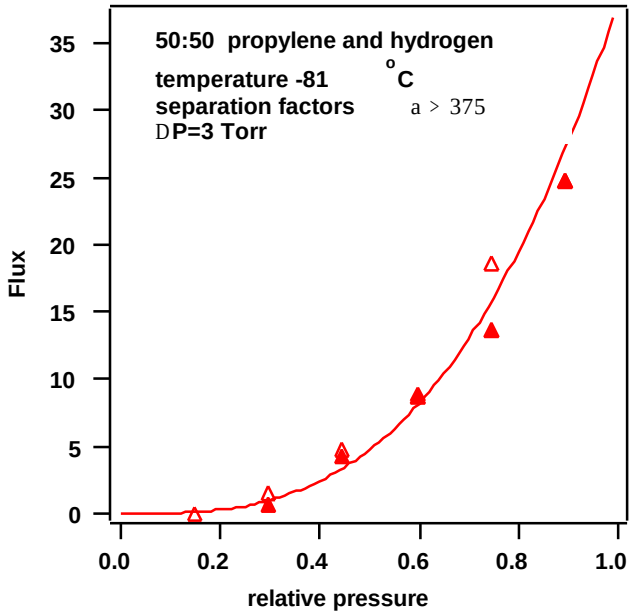

Fig. 8. Variation in propylene flux with pressure for 50 : 50 hydrogen/propylene gas mixture.

Transport through the membrane can be by Knudsen flow in the gas phase, surface diffusion of an adsorbed phase, or viscous flow of the condensate. For a fully condensed capillary, the overall hydrostatic pressure acting on the liquid can be significantly different from the applied pressure. Following Lee (5) by combination of the Kelvin and La Place equation, the approximate capillary pressure drop is given by:

$$\Delta P_c = \frac{RT\,\Delta P_g}{V\,P_m} \qquad (2)$$

ΔP_g is the gas pressure drop across the membrane, and P_m is the mean gas pressure. Equation 4 predicts that the pressure drop acting on the liquid can be several hundred times greater than the actual applied gas pressure drop. For the propylene/hydrogen system, a pressure drop of 3 torr results in an effective capillary pressure drop of 30 psi. For the description of viscous flow through a porous media via Darcy's equation, the permeability coefficient will contain this additional factor

$$J = \frac{K_d\,RT}{\eta\,VP_m}\,\frac{dP_g}{dl} \qquad (3)$$

where K_d is a constant, η is the liquid viscosity and the length of the pore. This effect can lead to a high flux through the membrane with a small pressure drop, again significant to the scaling of a process.

REFERENCES

1. A. G. Dirks and H. J. Leamy, "Columnar Microstructures in Vapor Deposited Thin Films," *Thin Solid Films* **47,** 219–33 (1977).
2. K. H. Muller, "Dependence of Thin Film Microstructure on Deposition Rate by Means of Computer Simulation," *J Appl. Phys.* **58**(7), 1 2573 (1985).
3. R. Messier, A. P. Giri, R. A. Roy, "Revised Structure Zone Model for Thin Film Physical Structure," *Vac Sci. Technol. A* **2**(2), 500 (1984).
4. D. Devlin, T. Archuleta, R. Barbero, N. Calamur, and M. Carrera, "Membrane Systems for Energy Efficient Separation of Light Gases," *Advanced Industrial Materials (AIM) Program: Annual Progress Report, FY 1997*, p. 135, 1997.
5. K. Lee and S. Hwang, "The Transport of Condensable Vapors through a Microporous Vycor Glass Membrane," *J. Colloid and Interface Sci*. **110**(2), 544 (1986).

MILESTONES DURING FY 1998

Membranes produced by oblique-angle sputter-deposition techniques have been tested for a number of systems. Systems consisting of gas mixtures of methane, ethane, propane, nitrogen, and proylene/hydrogen have been evaluated. Good separations have been obtained for tested systems along with exceptional fluxes.

PUBLICATIONS

D. Devlin, T Archuleta, R. Barbero, N. Calamur, and M. Carrera, "Membrane Systems for Energy Efficient Separation of Light Gases," *Advanced Industrial Materials (AIM) Program: Annual Progress Report*, FY 1997.

PRESENTATIONS

AIM Annual Meeting, Jacksonhole, Wyoming, June 1998.

HONORS AND REWARDS

None.

PATENTS/DISCLOSURES

David J. Devlin and Thomas Archuleta, "Membranes for Separation of Light Gases," Docket S-87-264, filed June 24, 1997.

N. Calamur and M. E. Carrera, "Energy Efficient Separation of Light Gases by Capillary Condensation," Docket 35,028, filed Disclosure, August 14,1995.

LICENSES

None.

INDUSTRIAL INPUT AND TECHNOLOGY TRANSFER

This effort will continue in FY 1999 as a joint research effort under the CRADA with Amoco Chemical Company. Amoco will develop characterization capabilities and design criteria for the membrane systems. With their guidance we will develop the materials and processing for the fabrication of these membranes. Amoco's goal is to scale this system for use in a pilot plant.

COST SHARING

Amoco will cost share with in-kind funds and capital investment exceeding the present DOE allocation.

ESTIMATED ENERGY SAVINGS

Initial economic analyses have shown that the commercialization of this novel separation concept could result in an energy-reduction potential of 5 trillion Btu per year for an olefins complex: this corresponds to a potential annual savings of nearly $8 million.

HIGHLIGHTS

A method for developing carbon pores for capillary condensation of hydrocarbons has been devised. Experiments demonstrate the separation of hydrocarbons using these membranes. Patents have been applied for.

New Method for Synthesis of Metal Carbides, Nitrides, and Borides

Rasit Koc, Geoffrey A. Swift, and Chang Meng
Department of Mechanical Engineering and Energy Processes
Southern Illinois University at Carbondale
Carbondale, Illinois 62901

INTRODUCTION

The objective of this project is to develop a new synthesis method using a carbothermic reduction reaction of carbon-coated precursors for producing high-purity, submicron, non-agglomerated powders of metal-carbide, metal-nitride, and metal-boride systems. A further objective is to demonstrate the advantages of the process and provide information on the applicability of the process for producing related advanced ceramic powders. During FY 1998, steps were taken to investigate the formation of TiC from carbon-coated precursors (kinetics of the reaction) and to understand the sintering behavior of resultant TiC powders using nickel. About 300 g of submicron TiC powders with desired properties have been produced and supplied to ORNL for testing and evaluation.

TECHNICAL PROGRESS FY 1998

Abstract

This technical report deals with the formation of titanium carbide from carbon-coated titanium dioxide precursors and the liquid-phase sintering with nickel of the as-produced TiC powder. This study makes use of differential scanning calorimetry (DSC), thermogravimetric analysis (TGA), X-ray diffraction (XRD), and both scanning and transmission electron microscopy (SEM and TEM). DSC curves of both coated and mixed 33.2 wt % carbon containing titania demonstrate the superiority of the coated precursor as it exhibits more reactions, at lower temperatures, than the mixed precursor. TGA data allowed for calculation of the activation energy of TiC. The activation energy was calculated as 731.6 kJ/mol. XRD characterized the products resulting from the reaction of both the mixed TiO_2-C and the carbon-coated TiO_2 for isotherms of each 100°C interval from 1100 to 1500°C, inclusive. These diffraction patterns support the hypothesis that the TiC formation proceeds through the formation of lower oxidation states of titanium. Liquid-phase sintering of TiC-Ni compacts, using submicron TiC produced with carbon-coated precursors (of carbon content from 30.95 to 34 wt %) and TiC from H. C. Starck, was performed to determine the effects of initial carbon content, sintering temperature, sintering atmosphere, and nickel content. The products from the submicron TiC-Ni compacts were compared with those of the Starck powder. The Starck powder compacts showed higher porosity and generally worse properties than their counterpart submicron powder compacts. The sintered Starck powder compacts also resulted in a third phase, identified through DSC as Ni_3Ti.

I. Background

Non-oxide ceramic materials generally have the advantages of high values for melting temperature, strength, oxidation resistance, and wear resistance, and a low thermal expansion coefficient. When all this is coupled with the general low mass density, the materials generate much excitement. Among these materials is titanium carbide (TiC).

Most ceramic parts are produced by sintering powders of the material. Sintering is a process by which the powders are raised to a temperature sufficient to cause mass transfer and densification. Sinterable powders, to be considered high quality, must meet the following five specific requirements: (1) be pure and single phase, (2) have a narrow size distribution, (3) be spherical in shape, (4) be submicron in size, and (5) be free of agglomerations. If these criteria are not met, the possibility of introducing a heterogeneity increases, which heterogeneity may propagate and generate others as production is carried out (1).

Industrial TiC production uses carbothermal reduction of titanium dioxide, TiO_2, in the presence of carbon, C, more than any other method. While this method produces large amounts of powder through the use of inexpensive precursors, the powders produced are generally of low quality (i.e., they do not satisfy all five powder characteristics mentioned above). Currently, no commercial powder-production process produces TiC powder of submicron size (2).

Folmer applied the carbon-coating process developed by Koc and Glatzmaier to produce a TiC powder that meets all of the above criteria (2–4). In order to demonstrate to industry the desirability of the coating process over conventional mixing processes, this study has been undertaken with the goal of determining the superiority of coated precursors to conventional mixed precursors, both in the formation of TiC and in the sintering of TiC-Ni compacts. Of large importance is the fact that TiC is a less expensive substitute for tungsten carbide, as WC requires cobalt as a binder for sintering, while TiC can use less expensive nickel as a binder (5).

The advantage of using coated precursors is the intimate contact achieved between reactants, while contact between reactants in conventionally mixed powders is haphazard at best, regardless of the mixing time used. Thermodynamic data do not consider lack of contact between reactants, while in fact this lack prevents reactions from occurring at their ideal thermodynamic temperatures. The intimate contact achieved using coated precursors allows the best possible chance for a reaction to proceed as per thermodynamic considerations.

The methods to be employed in determining the activation energy and reaction onset temperatures were TGA, DSC, and XRD. The activation energy of the TiC formation reaction was calculated from the TGA data for the coated precursor. DSC data from both mixed and coated TiO_2 precursors showed the occurrence of reactions, with the precursor exhibiting reaction(s) at lower temperature being superior. The products resulting from the reactions were characterized using XRD.

For sintering studies, TiC powders produced from coated precursors of 30.95 wt %, 32 wt %, and 34 wt % C were compacted with varying amounts of Ni. The same was done for TiC powder from H. C. Starck. Densification was carried out, with the resulting products being characterized by SEM. DSC was performed on TiC–20 wt % Ni compacts using TiC powder from 34 wt % C precursor and H. C. Starck. The DSC behavior indicated the temperature(s) of reactions occurring as each was reacted under argon.

II. Experimental Procedure

2.1 DSC and TGA of mixed and coated precursors

Both the mixed and coated precursors were prepared using submicron TiO_2 powder (P-25, Degussa Corp., Ridgefield Park, New Jersey), shown in Fig. 1, with surface area of 49.5 m^2/g. Note the relative state of agglomeration of the powders. Propylene gas, C_3H_6, was the source of carbon for the coated precursor, while carbon black (Monarch 880, Cabot, Waltham, Massachusetts) was used for the mixed precursor.

The coated precursor was prepared by cracking C_3H_6 gas at 600°C, with pyrolytic carbon coating the TiO_2. As this process has been proven to be surface-area activated, each TiO_2 particle is coated by a like amount of porous amorphous carbon (Fig. 2). Coating was continued until the TiO_2 had been coated to 33.2 wt % C. The mixed precursor was prepared by mixing appropriate amounts of TiO_2 and carbon for 60 min in a Spex Mixer/Mill (Model 8000, Spex, Meutucheen, New Jersey).

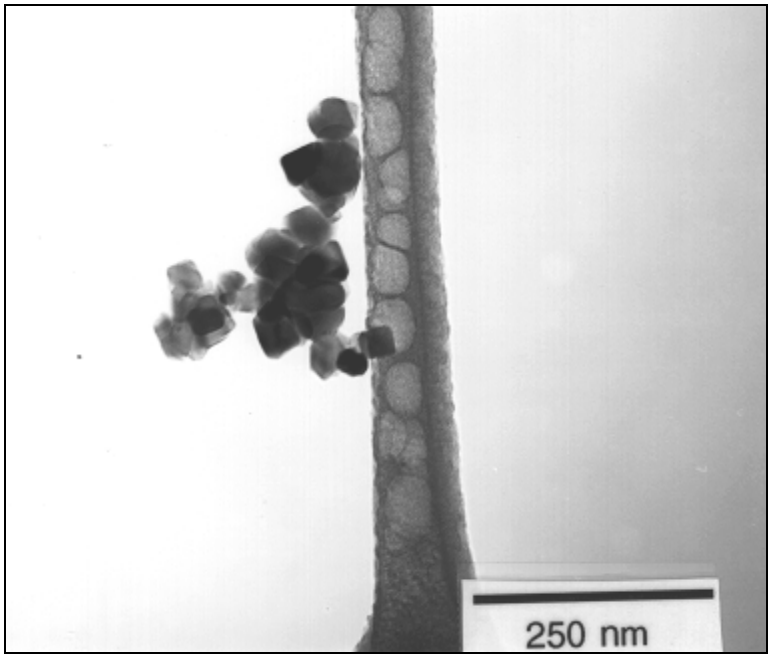

Fig. 1. TEM of Degussa P-25 TiO_2.

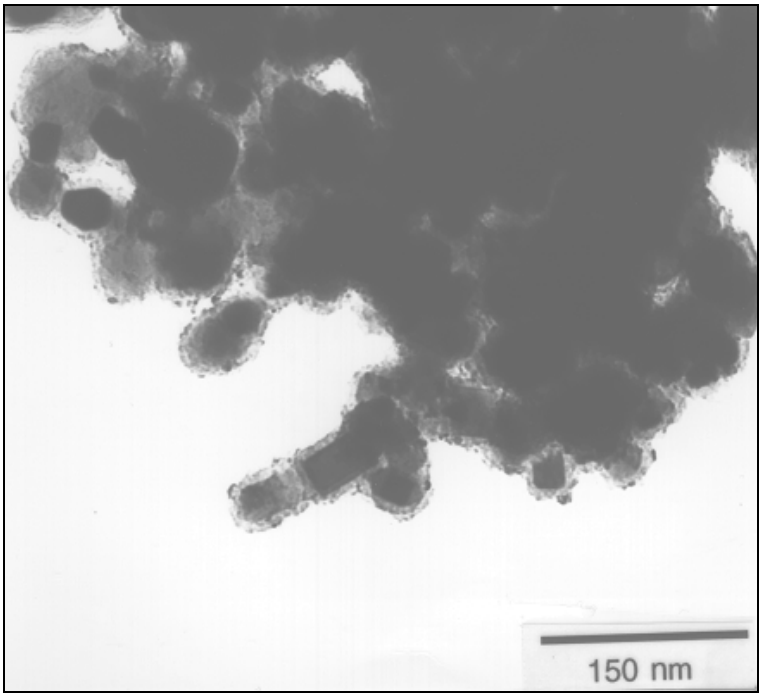

Fig. 2. TEM of 33.2 wt % carbon-coated P-25 TiO_2.

The overall carbothermal reduction reaction to be studied is:

$$TiO_2 + 3C \quad TiC + 2CO(g) \qquad (1)$$

Thermodynamically, reaction (1) occurs at 1289°C. However, the reaction is generally considered to proceed as the successive formation of lower oxides of titanium. The following possible reaction series, based upon Gibbs Free Energies, was proposed for this research:

$$4TiO_2 + C \rightarrow Ti_4O_7 + CO(g) \qquad (2)$$

$$3Ti_4O_7 + C \rightarrow 4Ti_3O_5 + CO(g) \qquad (3)$$

$$Ti_3O_5 + 8C \rightarrow 3TiC + 5CO(g) \qquad (4)$$

Reactions (2), (3), and (4) occur thermodynamically at 1087°C, 1182°C, and 1334°C, respectively. It is very likely that after reactions (2) and (3) occur, any as-yet unreacted TiO_2 will proceed at 1289°C as per reaction (1) with Ti_3O_5 following reaction (4) once 1334°C is reached.

DSC reactions used 15-mg samples of each precursor. The samples were heated in a Pt crucible at 20°C/min to 1500°C in flowing argon in a Setaram Labsys TG-DTA/DSC (Setaram Corp., Caluire, France). The DSC curves are shown in Fig. 3. The coated precursor exhibits three clear endothermic reactions, at 1192°C, 1310°C, and 1389°C.

Each reaction proceeds upon the completion of the previous reaction. The mixed sample shows reactions at 1274°C and 1379°C. This DSC data indicate that the coated precursor completes three reactions under 1400°C, with the initial reaction occurring at a lower temperature than for the mixed.

TGA was performed in the Labsys at isotherms of 1100°C, 1200°C, 1300°C, 1400°C, and 1500°C using a Pt crucible. Each isotherm was performed three times to ensure accuracy. The TGA weight-loss data were used to calculate the fraction converted, shown in Fig. 4. (Note: fraction converted = wt % lost/theoretical wt % loss. From stoichiometry, the theoretical wt % loss was calculated as 48.33 wt % from equation (1).) Next, the fraction converted data were used to calculate the activation energy according to the Arrhenius relation.

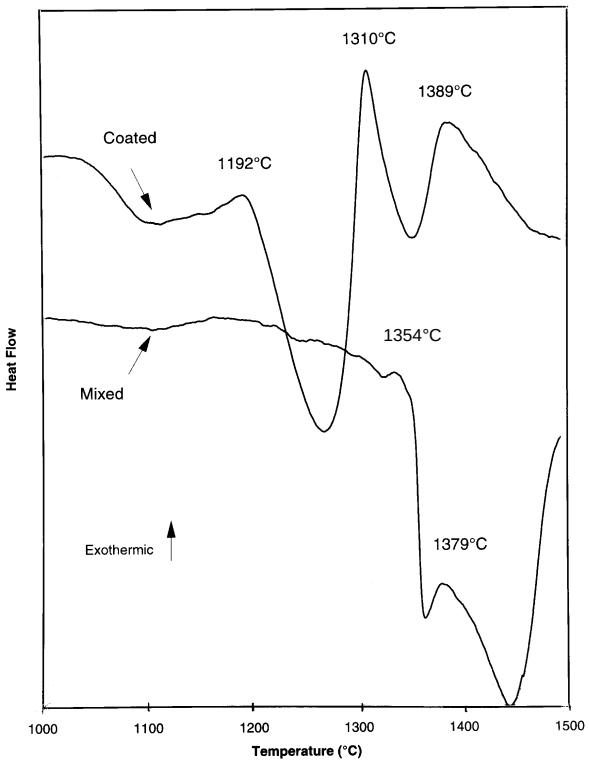

Fig. 3. DSC curves of mixed and coated TiO_2.

2.2 Sintering of TiC-Ni

Precursors were prepared per the coating method described above, each containing 30.95 wt %, 32 wt %, and 34 wt % carbon, respectively. A tube furnace (Model CTF 17/75/300, Carbolite, Sheffield) with an ID of 70 mm was used for TiC powder synthesis. Sixty grams of each precursor were placed in a graphite crucible (ID = 65 mm and length = 10 cm), then placed in the tube furnace. The tube was sealed, then evacuated, then purged with argon. A flowing stream of Ar at 1 LPM was supplied during the synthesis. The samples were heated at 4°C/min, held at 1550°C for 4 h, then cooled at 4°C/min.

The TiC powders thus produced were mixed with nickel in the Spex mixer. Wet milling of the powders in alcohol (30 ml) was performed in a tungsten carbide container with two tungsten carbide balls. After mixing for 2 h, the powder slurry was dried in a vacuum oven at 65°C. Uniaxial compaction was used to consolidate powders and form the green body. Small pellets were made by single-action pressing in a hardened-steel die (ID = 12.95 mm). Green bodies were produced at different pressures to get a green density between 45 and 65% theoretical density. [The theoretical density used was 5.724 g/cm^3, using 4.93 g/cm^3 for TiC density and 8.9 g/cm^3 for nickel density, calculated using exact ratios per the amount of each used in the mixing (i.e., 3 wt %, 5 wt %, 10 wt %, or 20 wt % Ni.).]

The pellets were densified in the same tube furnace used for TiC synthesis. First, pellets of TiC from each precursor with 20 wt % Ni were sintered at 1500°C for 2 h in flowing Ar + 10% H_2. The optimum carbon content was determined by density and shrinkage measurements, SEM, Vickers hardness, and fracture-toughness analyses. Next, pellets of the TiC powder with optimum carbon content were sintered with 3 wt %, 5 wt %, and 10 wt % Ni at 1500°C to determine the influence of Ni content. Next, compacts of the same TiC powder and 3 wt % Ni were sintered from 1300 to 1500 °C in flowing Ar + 10% H_2; this determined the effect of sintering temperature. A second sintering atmosphere, argon gas, was used for the sintering of TiC–3 wt % Ni to determine the influence of sintering atmosphere. Additionally, commercial TiC powders from H. C. Starck (HCS) were compared to the submicron TiC powders. For this purpose, HCS TiC pellets with Ni were sintered under similar conditions.

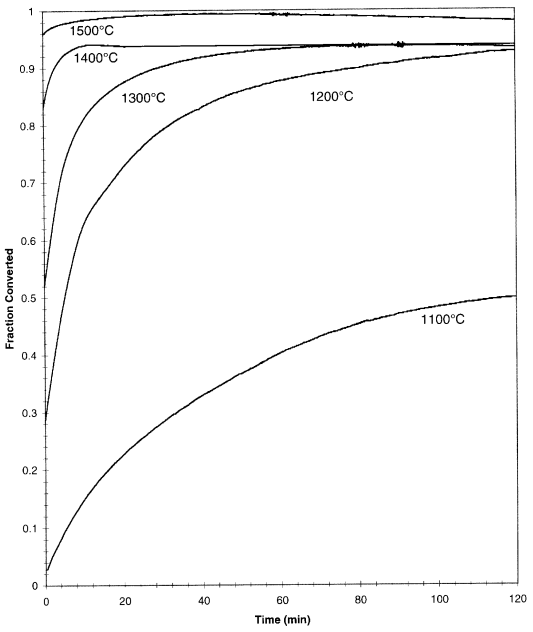

Fig. 4. Fraction converted for TGA isotherms of carbon-coated TiO_2.

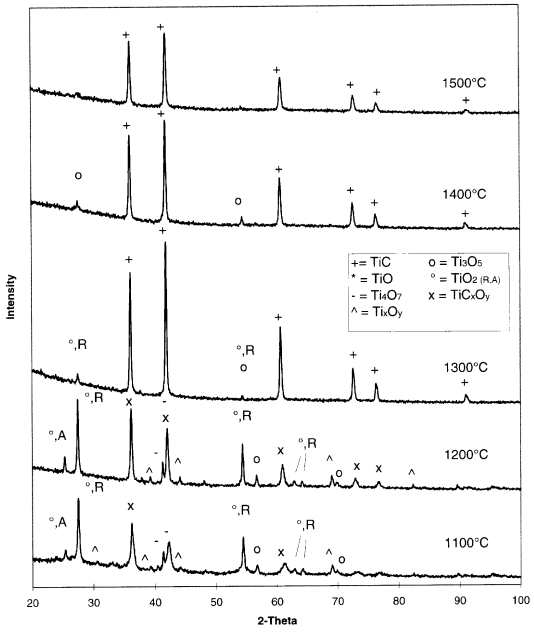

Fig. 5. XRD of reaction products from TGA isotherms of carbon-coated TiO_2.

III. Results and Discussion

3.1 XRD

XRD was performed on the products of each isotherm (Model DMAX-B, Rigaku, Tokyo, Japan). The diffraction patterns resulting are shown in Fig. 5. Each peak has a label serving as identification for the compound most likely to cause a peak at that 2-theta measure. Several peaks are of unknown composition, which may indicate the presence of some Magneli phases (6).

At 1100°C, the XRD pattern indicates very little in the way of TiC formation. There are two peaks for Ti_4O_7, which supports the earlier proposed reaction sequence. There are also several peaks for Ti_3O_5. The 1200°C pattern appears very similar to the 1100°C pattern. The differences are the increasing amplitude of the TiC_xO_y peaks, as the powder is reduced further due to the higher temperature. Also, the Ti_4O_7 peaks are decreasing in amplitude. Also present are the peaks of Ti_3O_5 or Ti_xO_y.

At 1300°C and 1400°C, TiC is the most prevalent compound. There are, however, the remnants of two titanium oxide peaks that each occur at 2-theta measures consistent with Ti_3O_5. At 1500°C, TiC is the only remaining product of sufficient quantity to cause diffraction peaks. All TiC_xO_y and Ti_xO_y peaks have been eliminated. Note the decreasing intensity of the peaks at 1400°C and 1500°C from the intensity at 1300°C. It is known that a decrease in peak intensity can be caused by increased grain size of the analyzed powder (7).

3.2 Activation energy for TiC formation

As the XRD patterns show, pure TiC has been formed. Thus it is possible to use the fraction-converted data to calculate the activation energy. For solid-state material reactions, the weight loss is equal to the fraction of reaction completed, α, as assumed for these calculations. Empirical studies have shown that

$$\frac{d\alpha}{dt} = k^n t^{n-1}(1-\alpha) \qquad (5)$$

applies to the isothermal kinetics of a variety of reactions, where t is time and k is the reaction rate constant (8). If k and t are assumed independent of α, then

$$\ln \frac{1}{1-\alpha} = (kt)^n \qquad (6)$$

$$\alpha = 1 - e^{-(kt)^n} \qquad (7)$$

(9,10). As k had to be calculated, equation (7) was transformed to:

$$\ln (1-\alpha) = -(kt)^n \qquad (8)$$

then

$$\ln[-\ln(1-\alpha)] = n \ln k + n \ln t \qquad (9)$$

When $\ln[-\ln(1-\alpha)]$ vs $\ln t$ is plotted, the slope is n and the y-intercept is $n \ln k$. The slope and y-intercept apply to straight-line fits of the fraction-converted data in the isothermal region, as in Fig. 4. Using the data obtained for $\ln k$ from the method just described (values shown in Table 1), plots of $\ln k$ vs t were prepared, and a straight-line fit applied to the data. According to the Arrhenius relation:

$$k = A e^{-\frac{E}{RT}} \qquad (10)$$

Transformation of equation (10) yields:

$$\ln k = \ln A - \frac{E}{RT} \qquad (11)$$

This equation is of the form, $y = mx + b$. By plotting $\ln k$ vs $1/T$, the slope is equal to the activation energy, E, divided by the Universal Gas Constant, R. Figure 6 shows $\ln k$ plotted vs $1000/T$. Using $R = 8.314$ J/mol K, with the slope value equal to –88,000 K, The value for E was calculated as 731.6 kJ/mol.

Table 1. Ln k vs T Values

Temperature (°C)	ln k
1100°C	–9.388
1200°C	–6.580
1300°C	–4.911
1400°C	1.320
1500°C	5.120

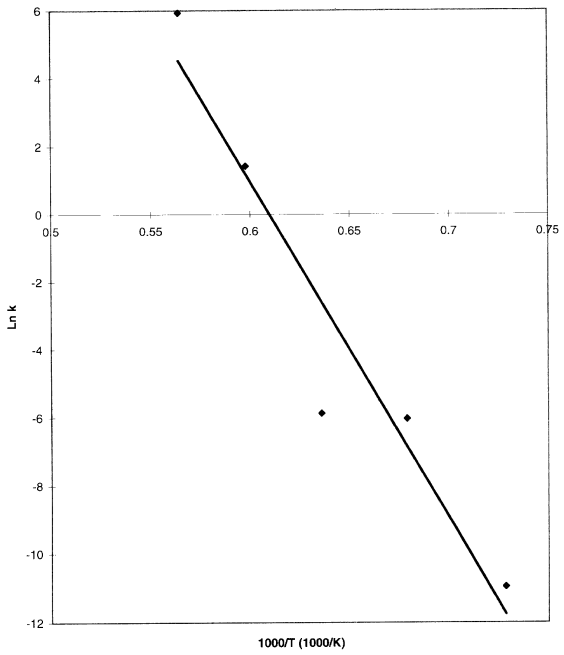

Fig. 6. Ln k vs 1000/T.

3.3 Sintering of TiC-Ni

3.3.1 Effect of precursor carbon content

Initial sintering studies were performed in flowing Ar–10% H_2 gas at a temperature of 1500°C using Ni as a binder. Table 2 shows the results of densification measurements of these pellets. It was observed that a higher degree of densification was obtained with lower carbon content. The sintered microstructure of compacts with 30.95 wt %, 32 wt %, and 34 wt % initial carbon content are shown in Figs. 7, 8, and 9, respectively. Liquid-phase distribution around TiC grains in the high carbon content sample was less uniform than in the sample with low carbon content. There is greater porosity in the higher carbon content compact. The TiC powders with 30.95 wt % initial precursor carbon content showed the best densification characteristics. This powder was thus determined to be that with optimum precursor carbon content.

Hardness measurements of TiC–20 wt % Ni according to initial carbon content are shown in Table 3. The cermet with the lowest carbon content exhibited the highest hardness, a finding which correlates with the presence of a larger percentage of hard, TiC, phase in the pellet. Also in Table 3, fracture-toughness values are shown for initial carbon content in the precursors. The change in fracture toughness as a function of carbon content followed a general trend similar to that of hardness.

Table 2. Densification Values as a Function of Precursor Carbon Content

Powder	Sintered Density (g/cm^3)	% TD (TD = $5.724 g/cm^3$)
TiC(30.95)	5.56	97
TiC(32)	5.10	89
TiC(34)	3.90	68
TiC(HCS)	5.53	96

Table 3. Vickers Hardness and Fracture Toughness Values as a Function of Precursor Carbon Content

Powder	Vickers Hardness (kg/mm^2)	Fracture Toughness (MPaÖm)
TiC(30.95)	1295	11.09
TiC(32)	1024	10.55
TiC(34)	219	7.9
TiC(HCS)	1189	10.99

Figure 10 shows a micrograph of TiC(HCS)–20 wt % Ni compact sintered under the same conditions. A high densification also was achieved after sintering. The titanium carbide particles were irregularly round and separated from each other by the nickel matrix. It was noted that TiC(HCS) particles are surrounded by a layer that is not found in the TiC(30.95)-Ni system. EDAX of this region indicated it to be of Ni_xTi_y composition.

Upon finding this new phase, DSC was performed to identify the composition. The DSC curves for the TiC(HCS) and TiC(30F) pellets, both with 20 wt % Ni, are shown in Fig. 11. The HCS pellet exhibited two endothermic reactions, while the 30F only one. The first reaction matches that of the 30F and was concluded to be the formation of the nickel liquid phase. The second reaction, based upon the reaction temperature and consultation of Ni-Ti phase diagram, was concluded to be the formation of Ni_3Ti, which has a eutectic near this temperature.

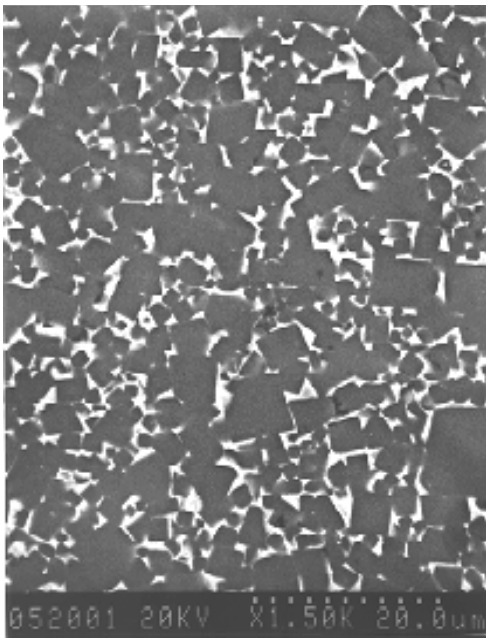

Fig. 7. SEM of sintered TiC(30.95)–20 wt % Ni.

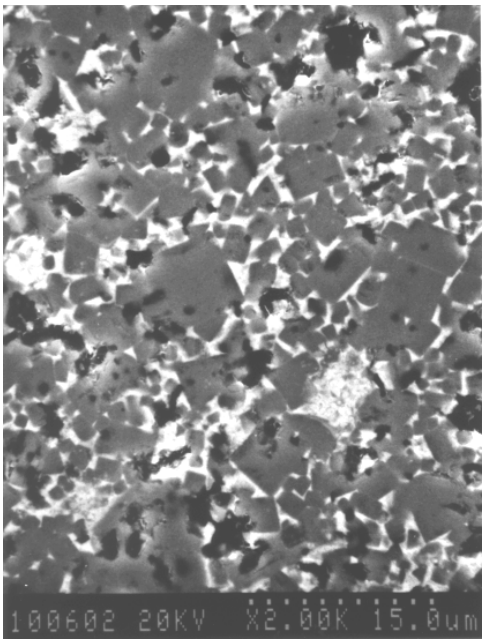

Fig. 8. SEM of sintered TiC(32)–20 wt % Ni.

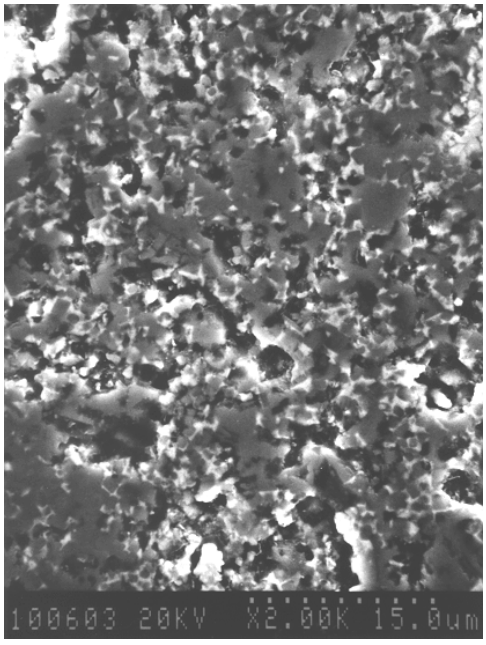

Fig. 9. SEM of sintered TiC (34)–20 wt % Ni.

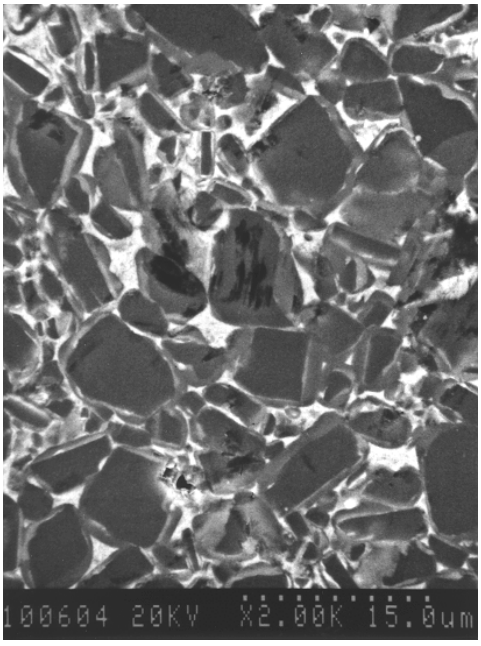

Fig. 10. SEM of sintered TiC(HCS)–20 wt % Ni.

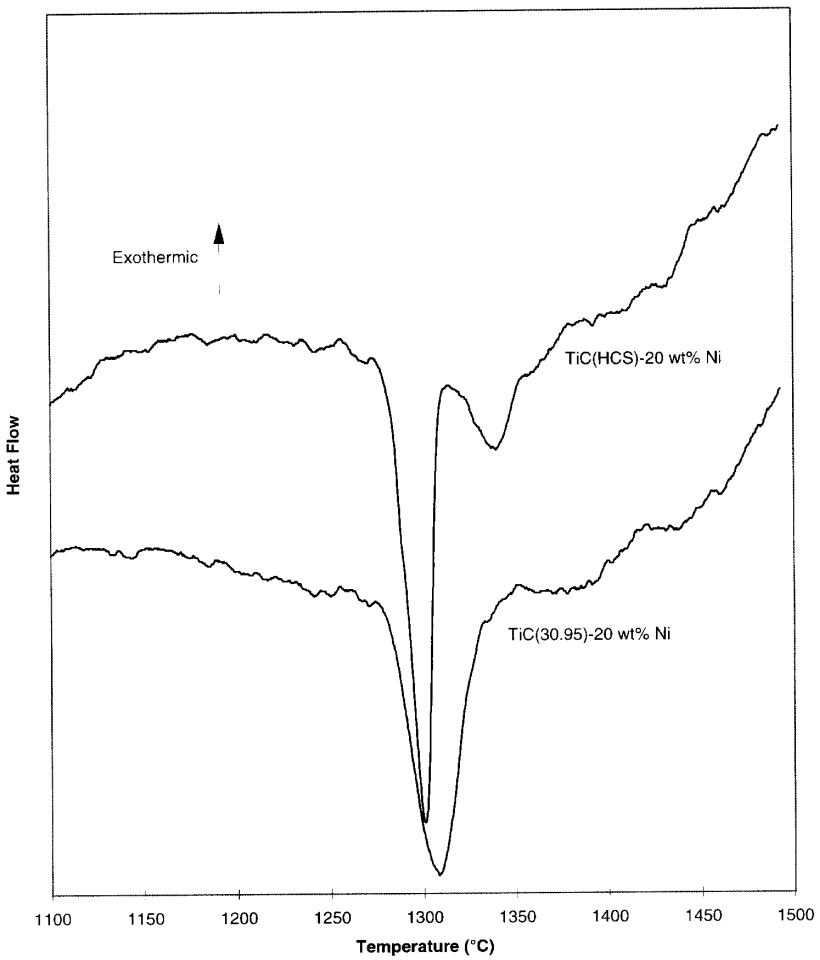

Fig. 11. DSC curves for TiC(34)–20 wt % Ni and TiC(HCS)–20 wt % Ni.

3.3.2 Effect of nickel content

TiC-based cermets are widely used as cutting tools and wear-resistant parts requiring high hardness; thus a smaller amount of Ni binder is preferred even though larger Ni content tends to increase fracture toughness (11). To determine the effect of Ni content on the densification of TiC(30.95)-Ni and TiC(HCS)-Ni systems, pellets were used with 20 wt %, 10 wt %, 5 wt %, and 3 wt % Ni. The densities of TiC(30.95) and TiC(HCS) with various amounts of nickel, sintered under the same conditions as before, are given in Table 4. Despite the nickel content variation, the sintered densities of TiC(30.95)-Ni composites exhibited a very small range of variance. An important observation of the TiC(30.95)-Ni system was that marked densification occurred with only low levels of Ni. However, the sintered densities of TiC(HCS)-Ni decreased considerably with the decrease of nickel content.

The hardness as a function of nickel content is shown in Table 5 for the TiC(30.95)-Ni and TiC(HCS)-Ni systems. The hardness of TiC(30.95)-Ni increased with decreased nickel content, as relatively more hard phase was present. The hardness of TiC(HCS)-Ni displayed a trend opposite to that of the TiC(30.95)-Ni composites. This behavior is attributed to increasing porosity in the structure with decreased nickel content. For all nickel contents, the TiC(30.95) samples had higher hardness than the corresponding HCS sample. The relation between the fracture toughness and the Ni content is shown in Table 6 for TiC(30.95)-Ni and TiC(HCS)-Ni systems. As expected, the fracture toughness decreased with decreasing Ni binder for the submicron powder. However, the fracture toughness of TiC(HCS)-Ni is higher than that of TiC(30.95)-Ni. This can be attributed to the testing method: the Vickers hardness indentation method depends on the crack length to determine fracture toughness. The presence of porosity inhibits crack propagation, leading to high fracture-toughness values. This, along with the third, Ni_xTi_y, phase, could account for the higher fracture toughness of the HCS samples.

Table 4. Densification Values as a Function of Nickel Content

Nickel Content (wt %)	TiC (30.95) (g/cm^3)	TiC (HCS) (g/cm^3)
3 (TD = 5.05)	5.01 (99% TD)	4.52 (89% TD)
5 (TD = 5.13)	5.14 (100% TD)	4.58 (89% TD)
10 (TD = 5.33)	5.33 (99% TD)	4.93 (92% TD)
20 (TD = 5.72)	5.56 (97% TD)	5.53 (96% TD)

Table 5. Vickers Hardness as a Function of Nickel Content

Nickel Content (wt %)	TiC (30.95) (kg/mm^2)	TiC (HCS) (kg/mm^2)
3	1750	797
5	1692	958
10	1546	1038
20	1295	1189

3.3.3 Effect of sintering temperature

To evaluate the effect of temperature on densification, TiC(30.95)–3 wt % Ni specimens were sintered under flowing Ar + 10% H_2 for 2 h at 1300°C and 1400°C, and compared with the earlier result at 1500°C. Table 7 shows the sintered densities of the specimens. Clearly, higher temperatures are essential for complete densification.

3.3.4 Effect of sintering atmosphere

The sintering atmosphere is also an important factor in liquid-phase sintering. Pellets of TiC(30.95)–3 wt % Ni and TiC(HCS)–3wt % Ni were sintered at 1500°C for 2 h under flowing Ar gas. Table 8 shows the influence of sintering atmosphere on densification. For TiC(30.95)–3 wt % Ni, the densification is higher under Ar than under Ar + 10% H_2, which is the opposite as for the HCS pellet. Previous researchers (12) have reported that TiC particles can be completely wetted by Ni in Ar atmosphere at 1500°C, but the contact angle is higher than 0° under H_2 atmosphere. The better wettability under Ar has resulted in the higher densification.

Table 6. Fracture Toughness as a Function of Nickel Content

Nickel Content (wt %)	TiC (30.95) (MpaÖm)	TiC (HCS) (MPaÖm)
3	5.35	8.69
5	5.69	9.33
10	6.78	7.9
20	11.04	10.99

Table 7. Densification Values as a Function of Sintering Temperature for Tic(30.95)–3 wt % Ni

Sintering Temperature (°C)	Sintered Density (g/cm^3)
1300	4.39 (87% TD)
1400	4.78 (94% TD)
1500	5.01 (99% TD)

Table 8. Densification Values as a Function of Sintering Atmosphere

Sintering Atmosphere	TiC (30.95)–3 wt % Ni Volume Shrinkage (%)	TiC (HCS)–3 wt % Ni Volume Shrinkage (%)
Ar + 10% H_2	42	30
Ar	43	29

Table 9 shows the hardness of TiC(30.95)–3 wt % Ni sintered under different atmospheres. The hardness of the sample sintered under Ar is slightly higher than that sintered under Ar + 10% H_2. This result can be attributed to the more uniform distribution of Ni liquid phase in the system, due to the atmosphere as described above.

Table 9. Vickers Hardness as a Function of Sintering Atmosphere for TiC(30.95)–3 wt % Ni

Atmosphere	Vickers Hardness (kg/mm^2)
Ar + 10% H_2	1719
Ar	1728

IV. CONCLUSION

Combining the use of TGA, DSC, and XRD, the formation of TiC by carbothermal reduction of carbon-coated TiO_2 clearly proceeds through the formation of lower oxides of titanium. The process first forms Ti_4O_7, then Ti_3O_5, with unknown TiC_xO_y and Ti_xO_y phases forming simultaneously. The reaction is essentially completed at 1300 °C, with higher temperatures providing the final purification into TiC. The activation energy for the formation of TiC using the carbon-coated precursor is 731.6 kJ/mol.

Submicron TiC powders were synthesized using carbon-coated TiO_2 precursors. The coated powders with higher carbon contents had finer particle size, looser agglomeration, and lower oxygen content than lower carbon content precursors, but the sintered pellets of these had worse densification, hardness, and fracture toughness than those of the lowest carbon content precursor. Ni content less than 20 wt % also results in the densification of the TiC-Ni system for both submicron TiC(30.95) and TiC(HCS) powders. However, the sintered density of submicron TiC(30.95) with low Ni content is much higher than that of TiC(HCS) with low Ni content. As nickel content is decreased for TiC(30.95)-Ni cermets, fracture toughness decreases and hardness increases, due to the increasing percentage of hard phase. The densification of TiC(30.95)–3 wt % Ni under Ar is slightly higher than under Ar–10% H_2, because of the change of wettability caused by the presence of hydrogen gas. Reduced Ni content causes higher porosity in the TiC(HCS)-Ni system; therefore, both fracture toughness and hardness decrease with decreasing Ni content. Because of the instability of TiC(HCS), oxygen could be picked up by H_2, leading to the higher density under Ar–10% H_2 than under Ar.

V. ACKNOWLEDGMENTS

Research performed at Southern Illinois University at Carbondale, sponsored by the U.S. Department of Energy, Assistant Secretary for Energy Efficiency and Renewable Energy, Office of Industrial Technologies, Advanced Industrial Materials Program, under contract DE-AC05-96OR22464 with Lockheed Martin Energy Research Corporation.

VI. REFERENCES

1. M. N. Rahaman, *Ceramic Processing and Sintering*, Marcel Dekker, Inc., New York, 1995.
2. R. Koc and G. Glatzmaier, "Process for Synthesizing Titanium Carbide, Titanium Nitride, and Titanium Carbonitride," U.S. Patent 5,417,952, 1995.
3. J. Folmer, Master Thesis from Southern Illinois University at Carbondale, "Synthesis of Titanium Carbide Using Carbon Coated Titanium Dioxide Precursors," 1996.
4. G. Glatzmaier and R. Koc, "Method for Silicon Carbide Production by Reacting Silica with Hydrogen Gas," U.S. Patent 5,342,494, 1994.
5. P. Ettmayer, "Hardmetals and Cermets," *Annu. Rev. Mater. Sci*., pp. 145–64 (1989).
6. L. M. Berger, "Titanium Carbide Synthesis from Titanium Dioxide and Carbon Black," *J. Hard Metals* **3**(1), 3–15, (1992).
7. B. D. Cullity, *Elements of X-Ray Diffraction*, 2nd ed., Addison-Wesley Publishing Company, Inc., London, 1978.
8. J. Burke, *The Kinetics of Phase Transformations in Metals*, Pergamon Press, London, 1965, p. 50.
9. W. F. Johnson and R. F. Mehl, "Reaction Kinetics in Processes of Nucleation and Growth," *Trans. AIME* **135**, 416, (1939).
10. M. Avrami, "Kinetics of Phase Change: I," *J. Chem. Phys*. **7**(12), 1103–12 (1939).
11. K. J. A. Brookes, *World Directory and Handbook of Hard-Metals*, 2nd ed., *Engineers' Digest*, London, 1979.
12. Ju. V. Naidich, "The Wettability of Solids by Liquid Metals," *Progress in Surface and Membrane* **14**, 441 (1981).

PUBLICATIONS

Journal

Rasit Koc and Swaroop Kaza, "Synthesis of α-Si_3N_4 from Carbon Coated Silica by Carbothermal Reaction and Nitridation," *J. Eur. Ceram. Soc.* **18**(10), 1471–77, 1998.

Rasit Koc and Sai Cattamanchi, "Synthesis of Beta Silicon Carbide Powders Using Carbon Coated Fumed Silica," *J. Mater. Sci.* **33**, 2537–49 (1998).

Rasit Koc, "Kinetics and Phase Evolution During Carbothermal Synthesis of Titanium Carbide from Ultrafine Titania/Carbon Powder Mixture," *J. Mater. Sci.* **33**, 1049–55 (1998).

Rasit Koc, "Kinetics and Phase Evolution During Carbothermal Synthesis of Titanium Carbide from Carbon-Coated Titania Powder," *J. Euro. Ceram. Soc.* **17(**11), 1309–15 (1997).

Rasit Koc and Jeffrey S. Folmer, "Carbothermal Synthesis of Titanium Carbide Using Ultrafine Titania Powders," *J. Mater. Sci.*. **32(**12), 3101–11 (1997).

Rasit Koc and Jeffrey S. Folmer, "Synthesis of Submicron Titanium Carbide Powders," *J. Amer. Ceram. Soc.* **80(**4), 952–56 (1997).

Rasit Koc and Jeffrey S. Folmer, "Synthesis of Titanium Carbide Powders Using Carbon Coated Titanium Dioxide Precursor," *Amer. Ceram. Soc. Transactions* **79**, 19–26 (1996).

S. Cattamanchi and R. Koc, "Synthesis of Submicron SiC Powders," *Ceramic Engineering & Science Proceedings of ACS Meeting on Composites, Advanced Ceramics, Materials and Structures-B* **18**(4), 695–703, 1997 (refereed).

Rasit Koc, "Kinetics and Phase Evolution During Carbothermal Synthesis of TiC," *Ceramic Engineering & Science Proceedings of ACS Meeting on Composites, Advanced Ceramics, Materials and Structures-B* **18**(4), 703–13, 1997 (refereed).

Presentations

Rasit Koc, "New Method for Synthesis of Metal Carbides, Nitrides, and Carbonitrides," *Materials Research Symposium, Materials Technology Center*, SIUC, April 30–May 1, 1998.

S. Kaza and R. Koc, "Carbothermal Synthesis of α-Si_3N_4 Powders from Carbon Coated Silica," presented at *ACS 100th Annual Meeting*, Paper No. SXI-054-98, Cincinnati, Ohio, May 3–6, 1998.

C. Meng and R. Koc, "Liquid Phase Sintering of Submicron TiC Powders Using Ni," presented at *ACS 100th Annual Meeting*, Paper No. SXVP-008-98, Cincinnati, Ohio, May 3–6, 1998.

R. Koc, "Synthesis of Submicron TiC Powders Using Carbon Coated TiO_2 Precursors," *Advanced Ceramics for the New Millenium*, Atlanta, Georgia, March 12, 1998.

R. Koc, S. Cattamanchi, and S. Kaza, "Synthesis of Submicron Silicon Nitride Powders," presented at *ACS 99th Annual Meeting*, Paper No. SIII-003-97, Cincinnati, Ohio, May 4–7, 1997.

S. Cattamanchi and R. Koc, "Carbothermal Synthesis of β-SiC Powders Using Carbon Coated Colloidal Silica," presented at *ACS 99th Annual Meeting*, Paper No. SIII-028-97, Cincinnati, Ohio, May 4–7, 1997.

S. K. Kodambaka and R. Koc, "Synthesis of Submicron Tungsten Monocarbide Using a Novel Tungsten Trioxide Precursor," presented at *ACS Meeting on Composites, Advanced Ceramics, Materials and Structures*, Paper No. Si-0034-97F, Cocoa Beach, Florida, January 12–16, 1997 (Abstract Book, p. 34).

R. Koc and S. Cattamanchi, "Synthesis of Submicron SiC Powders," presented at *ACS Meeting on Composites, Advanced Ceramics, Materials and Structures*, Paper No. Si-0035-97F, Cocoa Beach, Florida, January 12–16, 1997 (Abstract Book, p. 34).

HONORS AND AWARDS

R&D 100 for the development of Method for Making Silicon Carbide Powder, award-winning team: R. Koc, G. C. Glatzmaier, K. Scholl, M. Anselma, and J. Sibold (1995).

Federal Laboratory Consortium Award for Technology Transfer, award-winning team: R. Koc, G. C. Glatzmaier, K. Scholl, M. Anselma, aand J. Sibold (1996).

Sigma Xi Research Award, Rasit Koc (1998).

PATENTS/DISCLOSURES

R. Koc and G. Glatzmaeir, "Process for Synthesizing Titanium Carbide, Titanium Nitride and Carbonitride," U.S. Patent 5,417,952.

R. Koc and S. K. Kodambaka, "Process for the Production of Tungsten or Tungsten Monocarbide Powders," ROI (1996).

LICENSES

ART Inc. licensed the SiC patent.

Greenleaf, Teledyne Metal Working Group, and Kennametal Inc. are interested in licensing TiC/WC technology.

INDUSTRIAL INPUT AND TECHNOLOGY TRANSFER

Greenleaf Corporation: The personnel at Greenleaf have been evaluating our TiC powders for their applications.

Oak Ridge National Laboratory (ORNL): The personnel at ORNL have a TiC-intermetallic composite program that is directed at developing composites with properties more superior for cutting-tool applications than the WC-Co currently in use.

ESTIMATED ENERGY SAVING

This technology will improve energy efficiency when compared to the conventional ones because it does not require high reaction temperatures for production of these powders.

LIST OF TABLES

LIST OF FIGURES

Synthesis and Processing of Composites by Reactive Metal Penetration

Ronald E. Loehman and Kevin G. Ewsuk
Advanced Materials laboratory
Sandia National Laboratories
Albuquerque, New Mexico 87185

Sylvia M. Johnson and Yigal Blum
SRI International
333 Ravenswood Ave.
Albuquerque, New Mexico 87106

William G. Fahrenholtz
Advanced Materials Laboratory
University of New Mexico
Menlo Park, California 94025

Donald T. Ellerby*
Advanced Materials Laboratory
Sandia National Laboratories
Albuquerque, New Mexico 87106

*On leave from the University of Washington, Seattle, Washington.

INTRODUCTION

The historical development of the modern industrial world is based in many ways on continuous improvements in available engineering materials. Remarkable increases in materials properties have been achieved through better understanding and control of composition and microstructure. Demands for further improvements or for combinations of properties that are unattainable in single-phase materials are leading researchers increasingly to focus their attention on composite materials. Ceramic-metal composites, for example, are better than monolithic materials for many applications because of their high stiffness-to-weight ratios, good fracture toughness, and excellent high-temperature stability. Their electrical and thermal properties also can be varied through control of their compositions and microstructures. However, despite a lot of development effort, ceramic composites are still too expensive for most applications, and they have not demonstrated sufficient reliability for commercial use. There undoubtedly is a substantial market for structural composites if they can be made with reproducible properties by techniques that are affordable.

The project currently has been doing research and development work on a novel method for making ceramic-metal composites using reactive metal penetration of dense ceramic preforms. Our previous results have shown that reactive metal penetration addresses the two critical issues listed above: (1) economical processing through near-net-shape forming and (2) reproducibility of properties through control of compositions and microstructures. Making parts to near net shape is more economical because it reduces the costly and energy-intensive grinding and machining operations, and it minimizes finishing wastes. This makes reactive metal penetration attractive as an economical process for making the advanced ceramic composites that are needed for many industrial applications. Our most

promising composite compositions to date consist of Al and Al_2O_3 or Al, Al_2O_3, and $MoSi_2$.

One spin-off of this work is gaining a deep understanding of reactions between molten metals and ceramics. Promotion of reactions leads to composite material applications. Knowing how to minimize metal-ceramic reactions leads to such applications as refractories, containers, and die materials for the metal-processing industries. Whether for the composites themselves or for the insight it gives into improving refractories, this work should be of particular interest to the aluminum industry and the suppliers of the refractories used in aluminum processing.

The goals of this research and development project are:

- To identify compositions favorable for making composites by reactive metal penetration;
- To understand the mechanism(s) by which these composites are formed;
- To control and optimize the process so that composites and composite coatings can be made economically; and
- To apply the R&D results to problems of interest to industry.

Over the past 3 years the program has had a second part, which is performed under subcontract by SRI International. The SRI effort is concerned with making composite coatings, especially corrosion-resistant coatings on metals, by pyrolysis of preceramic polymers blended with metal or ceramic powders. Those coatings have advantages in engineering applications because they can protect such metals as aluminum and mild steel from corrosive and oxidizing environments. In addition, they are stable at high temperatures and may increase surface hardness. The preceramic polymer serves both as a high-temperature polymeric binder and, after pyrolysis, as a ceramic matrix. The composite coatings are applied by such simple deposition techniques as brushing, spraying, rolling, or dipping. The technique is a relatively low cost way to make durable coatings, but it requires further development to improve the processing conditions and coating uniformity and to evaluate properties.

The goals of the preceramic polymer research effort are:

- To identify feasible compositional systems for making composite coatings with good corrosion resistance;
- To evaluate the corrosion resistance in severe environments; and
- To optimize formulation, deposition, and curing processes, especially low-temperature processes.

TECHNICAL PROGRESS IN FY 1998

Summary

Reactive metal penetration (RMP) has several characteristics that make it an attractive technique for synthesis of structural composites. Preforms of dense aluminosilicate ceramics with the desired size and shape of the final part are made by any of the common, inexpensive ceramic-processing techniques. The preform is then immersed in molten aluminum, which initiates reaction and conversion to the composite part with no change in size or shape. The reaction for the simplest case can be written as:

$$(8 + x)\ Al + 3\ Al_6Si_2O_{13} \rightarrow 13\ Al_2O_3 + 6\ Si + x\ Al \qquad (1)$$

The composite formation rate varies with temperature and, in the optimum range of 1050 to 1200°C, is rapid and increases linearly with time. Conversion rates of 5 mm/h are achieved, which compares very favorably with formation rates for other high-temperature materials. In previous work, we developed a mechanistic model for composite formation that explains its important features: (1) the rapid, linear kinetics of formation for temperatures below about 1200°C; (2) the decrease in reaction rate above 1200°C; and (3) the effect of Si concentration in the Al on reaction kinetics. Development of the model depended on detailed microstructural information from transmission electron microscopy (TEM) studies done in collaboration with Professor Ping Lu of New Mexico Tech. This result was published recently [W. G. Fahrenholtz, K. G. Ewsuk, R. E. Loehman, and P. Lu, "Kinetics of Ceramic-Metal Composite Formation by Reactive Metal Penetration," *J. Amer. Ceram. Soc.* **81**(10) 2533–41 (1998)]. One practical consequence of our model is that it has allowed us to construct a process diagram showing the time-temperature combinations where the RMP reaction between aluminum and mullite has favorable rates.

Alternative composite systems

A major challenge in advanced materials is to optimize the properties of a component for a specific application. Optimization may require tradeoffs in materials properties, which frequently is accomplished through changes in composition or microstructure of the material. For example, in applications requiring exposure to hostile environments, strength or toughness may be sacrificed for improved corrosion resistance. For most composite systems, even minor changes in the composition or microstructure of the composite require major alterations in processing conditions, which can add significantly to costs. One of the advantages to RMP and reactive hot pressing (RHP) is the ability to modify the composition of the final composite by changing only the precursor, without altering the processing conditions. An example is the range of metal phases obtainable in alumina-metal composites by varying only the ceramic preform composition. For example, either Nb-alumina or Ni–alumina composites can be made by the same process, depending only on whether the preform contains Nb_2O_5 or NiO. The same mixing method, handling, and hot-pressing conditions are used for both compositions, but one gives an Al_2O_3-Ni composite, whereas the other produces Al_2O_3-Nb. In some cases, the microstructure also can be manipulated by simple changes in the process cycle, such as altering the heating

rate. In the case of Al_2O_3-$MoSi_2$ composites, the morphology of $MoSi_2$ inclusions can be changed from equiaxed to elongated (along with a substantial increase in strength) by decreasing the heating rate during hot pressing from 10°C/min to 1°C/min.

Toughening RMP composites

As discussed in previous reports, metal-reinforced ceramic composites offer the potential for improvements in toughness and reliability compared with monolithic ceramics. Equation 1 above shows that Si is produced as a by-product of the RMP reaction. Most of the Si that results from the reaction diffuses into the surrounding Al bath with a counter diffusion of Al into the composite. Recent work has shown that both the strength and toughness are influenced by the amount of Si retained within the composite. Using RMP, the volume fraction of metal in the composite can be varied either by altering the Al_2O_3 : SiO_2 ratio in the preform or by varying the volume fraction of porosity in the preform. Recently, we have made composites with precise metal contents using preforms made from mullite powder doped with colloidal silica. Using these preforms we were able to make composites with the desired 25 and 30 vol % metal. Thus, we are able to accurately vary the composite metal content by carefully controlling the preform composition. Controlling the metal volume fraction and processing to remove Si from the composite results in microstructures with metal ligaments that can bridge any cracks that might develop in use. This type of microstructure improves ceramic reliability and results in an increasing toughness with increasing crack length that is known as resistance-curve or R-curve behavior.

Composite ceramic coatings

Low-cost preceramic binders mixed with a broad range of fillers can be applied to metals as composite coatings that adhere well and are very corrosion resistant. The concept is based on the use of a mixture of preceramic polymers, ceramic powders, and metal powders that react after heating to make durable coatings. Such formulations, when heated above 450°C, yield ceramic or metal/ceramic composite coatings, some with near zero shrinkage. At lower temperatures, an inorganic-organic hybrid material (90% and above is inorganic) coating is formed from the highly cured polymer and the filler powders. When applied to aluminum, steel, and other metals, these coatings are very adherent, withstand wear, and are thinner than coatings from conventional, corrosion-resistant paints. In addition, VOCs are reduced and the coatings are resistant to HCl and long-term, salt-spray exposure.

Detailed Description of Technical Progress

The following detailed descriptions of results obtained in fiscal year 1998 are organized according to project tasks.

Task 1: Evaluate reactions and mechanisms of composite formation in the Al/Mullite system.

Extensive previous work on this project has elucidated the kinetics and fundamental reaction mechanisms that control formation of composites by reactive metal penetration. Work under Task 1 in this fiscal year primarily has been to write up the results and submit them for publication. This has culminated in the following submissions: (a) W. G. Fahrenholtz, K. G. Ewsuk, R. E. Loehman, and P. Lu, "Kinetics of Ceramic-Metal Composite Formation by Reactive Metal Penetration," *J. Amer. Ceram. Soc.* **81**(10) 2533–41 (1998); (b) W. G. Fahrenholtz, D. T. Ellerby, K. G. Ewsuk, and R. E. Loehman, "Calculation and Control of Compositions of Al_2O_3-Al Composites by Reactive Metal Penetration of Dense Aluminosilicate Preforms," submitted; (c) P. Lu, T. B. Du, R. E. Loehman, K. G. Ewsuk, and W. G. Fahrenholtz, "Interfacial Microstructure Formed by Reactive Metal Penetration of Al into Mullite," submitted; and (d) W. G. Fahrenholtz, B. P. Hansen, K. G. Ewsuk, and R. E. Loehman, "Forming Al_2O_3-Al-Si Composites by Combined Physical Infiltration and Reactive Metal Penetration of Porous Aluminosilicate Preforms," submitted.

Impact. Understanding the mechanism that controls the kinetics of composite formation and the effects of process variables on microstructure and properties allows us to make parts that are reproducible and that can be optimized for specific applications. Because we know the effects of changes in process variables on the properties of the resulting composites, we can design more robust manufacturing cycles that make the composites more amenable to commercial production.

Future work. The present RMP process exhibits much more rapid formation rates than other reactions between liquids and dense solids. One question we plan to investigate is how widespread is the mechanism that gives such rapid rates. Similarly rapid composite formation in other compositions would be of considerable commercial importance.

Task 2: Evaluate other ceramic-metal systems

As discussed in previous reports, we have prepared $MoSi_2$-Al_2O_3 composites by reacting Mo, Al, and mullite powders following Reaction 2.

$$3\ Mo + 8\ Al + 3\ Al_6Si_2O_{13} \rightarrow 13\ Al_2O_3 + 3\ MoSi_2 \qquad (2)$$

This composite is remarkable for the high four-point bend strength it achieves, 470 MPa, with a relatively low content (~20 vol %) of $MoSi_2$. Other composite compositions with different stoichiometries of the reinforcing intermetallic phase can be prepared by adjusting the ratios of the starting materials. For example, to increase the intermetallic content of the composite, extra Mo and Al can be incorporated into the batch, resulting in composites that contain up to 50 vol % of the intermetallic. However, the intermetallic phase in these composites is $Mo(Si,Al)_2$ or Mo_3Al_8, rather than $MoSi_2$. To increase the $MoSi_2$ content of the composite, other ceramic precursor powders must be used. Composites containing

~30 and ~40 vol % $MoSi_2$ can be formed by substituting calcined kaolin or silica for mullite, according to Reactions 3 and 4.

$$3\ Mo + 8\ Al + 3\ Al_2Si_2O_7 \rightarrow 7\ Al_2O_3 + 3\ MoSi_2 \quad (3)$$

$$3\ Mo + 8\ Al + 6\ SiO_2 \rightarrow 4\ Al_2O_3 + 3\ MoSi_2 (4)$$

However, when powders batched according to Reactions 3 and 4 are hot-pressed using standard reaction conditions (10°C/min heating rate to 1450°C, apply 5000 psi, and hold 30 min), the composites produced are porous and have bend strengths of only 210 MPa. The increase in porosity is attributed to segregation of the aluminum after it melts but before it has time to react. Segregation delays reaction to 1000°C (as detected by DTA), which produces relatively large particles of $MoSi_2$ in the composites.

Segregation of aluminum prior to reaction must be minimized to prepare composites with $MoSi_2$ contents higher than 20 vol % and high relative densities. Claussen and co-workers have shown that reactions involving finely divided aluminum can be controlled by using heating rates as low as 1°C/min. They use slow heating rates to promote controlled reactions at relatively low temperatures to make reaction-bonded aluminum oxide (RBAO) and to form metal-ceramic composites by their 3A process. To investigate the effects of heating rates on our system, we sintered pellets made from mixtures of finely divided Mo, Al, and kaolin powders under vacuum or argon at rates of 10°C/min or 1°C/min. The higher heating rate always resulted in bloated pellets that broke into several pieces during reaction. The lower heating rate produced uniform pellets that remained whole, although they did not achieve full density. Examination by DTA showed that a 10°C/min heating rate leads to an aluminum melting endotherm at 660°C and the composite-forming reaction at ~1000°C. However, when a heating rate of 1°C/min was used, no aluminum melting endotherm was observed, and the composite-forming reaction occurred at a much lower temperature, around 850°C. The DTA results suggest that the reduction in reaction temperature is due to increased homogeneity in the precursor that allows the Al to react below its melting point. If there are no large particles to melt, they cannot segregate prior to reaction. The segregation presumably is driven by the fact that molten aluminum does not wet most ceramics, favoring the formation of large drops rather than fine, dispersed ones.

Mo-Al-kaolin powder mixtures were hot-pressed using a 1°C /min heating rate. The resulting composite had a higher density than that of composites produced using a 10°C/min heating rate, specifically 97% relative density for the 1°C/min sample compared with 92% for the 10°C/min heating rate. The lower heating rate also produced differences in the composite microstructure. Composites produced using 10°C/min heating rates had relatively large, equiaxed $MoSi_2$ inclusions. In contrast, composites made using 1°C/min heating rates had elongated $MoSi_2$ regions, much like those in the high-strength composites containing ~20 vol % $MoSi_2$ that were prepared by hot-pressing Mo, Al, and mullite. The increase in density and the refinement of the microstructure suggest that composites with 30 vol % $MoSi_2$ made with 1°C/min heating rates may have much higher strengths than similar compositions produced using a 10°C/min heating rate (210 MPa).

Mechanical test specimens are being made from composites prepared with the 1°C /min heating rate.

The slower 1°C/min heating rate also was used for synthesis of Al_2O_3-Ni composites according to Reaction 5:

$$2\ Al + 3\ NiO \rightarrow Al_2O_3 + 3\ Ni \qquad (5)$$

This composite has been difficult to prepare due to macroscopic phase segregation during reaction when a 10°C/min heating rate was used. Typically, because of poor wetting of the NiO, once the Al melts, it wicks to the outer surface of the pellet. This produces specimens in which the Al_2O_3 is segregated to the outside as a porous shell around a Ni core. When reacted using the 1°C/min heating rate, the Al-NiO powder yielded dense, homogeneous Al_2O_3-Ni composites. By reducing the heating rate to 1°C/min, a uniform two-phase composite was produced that had a fine-scale, interpenetrating microstructure. Figure 1 shows a SEM micrograph of a composite prepared by reacting Al and NiO using a 1°C/min heating rate. From Fig. 1, the average Ni ligament size in the composite is seen to be less than 5 µm. Mechanical test specimens were cut from hot-pressed billets. Four-point bend testing showed that the composite had an average strength of 610 ± 27 MPa. By comparison, the strongest Al_2O_3-Al composite prepared by RMP has a value of 410 MPa for a composite containing 26% Al. The hardness of the Al_2O_3-Ni composite was 5.4 ± 0.6 GPa.

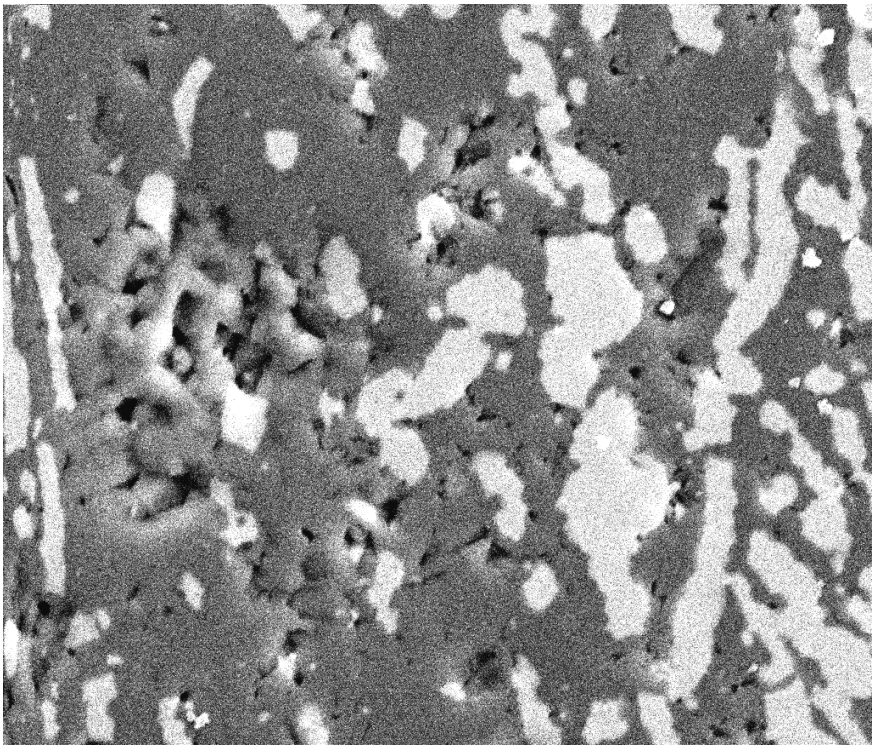

Fig. 1. SEM micrograph of an alumina-Ni composite prepared by hot-pressing Al-NiO powder mixtures with a heating rate of 1°C/min.

Impact. The demonstration that heating rate can be used to control reaction rate in composite formation is an important development. First, it allows us to prepare dense, high-strength composites with compositions that were previously inaccessible. These compositions include Al_2O_3-$MoSi_2$, Al_2O_3-Ni, Al_2O_3-Cu, and many others. Second, it gives us a method for controlling reactions that may allow us to produce composites by reactive pressureless sintering rather than reactive hot pressing. Previous attempts at reactive sintering have failed because the sintering and reaction could not be controlled independently. Simultaneous reaction and sintering produce porous composites.

Future Work. We are re-examining several composite systems to take advantage of this increased control over reaction rate. It should be possible to prepare dense composites in systems such as Al_2O_3-Cu and Al_2O_3-Nb that previously were impossible. We also are preparing mechanical test specimens to evaluate the strength, hardness, and toughness of the 30 vol % $MoSi_2$ composite and the Al_2O_3-Ni composites.

Task 3: Evaluate ceramic-metal composite microstructure and properties

Some of the Si produced in Reaction (1) above stays in the composite and does not diffuse out into the surrounding Al bath during processing. This residual Si has been shown to play a significant role in the mechanical properties of RMP composites. Consider, for example, results from two composites with 18 vol % Al formed by the reaction of Al with mullite. Both composites experienced identical initial reactions, but the second composite was subjected to a secondary heat treatment in contact with fresh Al in order to draw out as much of the residual Si as possible. X-ray diffraction analysis showed this second exposure to molten Al significantly reduced the residual Si content in the samples. Furthermore, the strength of the composite with reduced Si increased from 313 to 346 MPa compared to the samples exposed only once to molten Al, and their toughness increased from 4.1 to 5.0 $MPam^{1/2}$. Thus, the mechanical properties of RMP composites can be improved by reducing the residual Si within the metal phase.

The most significant factor limiting the use of ceramics as structural materials is their low reliability, which is caused by their high sensitivity to flaws. One way to improve ceramic reliability is by incorporating metal reinforcements; during crack propagation, the metal ligaments bridge the crack faces, thereby creating closing forces across them. This results in an increasing toughness with increasing crack length that is known as resistance-curve or R-curve behavior. It has been theorized that materials with steep R-curves (i.e., those that reach their plateau toughness over a short increase in crack length) will show reduced flaw sensitivity and improved reliability. Figure 2 shows measured R-curves for both of the composites with 18 vol % metal discussed above, that is those that underwent a secondary heat treatment to remove the residual Si and those that did not. Both of the samples have relatively steep R-curves that plateau after 300 to 500 μm of crack growth. Consistent with the previous discussion, we see that the heat-treated composite (with bridging ligaments) has a higher plateau in toughness than the untreated material (no bridging ligaments).

Figure 3 compares the R-curves for samples with 18 and 25 vol % metal, both of which were heat-treated to remove the residual Si. As expected, the plateau toughness increases (from 5 to 7 $MPam^{1/2}$) with increasing metal content. Both R-curves are relatively steep and plateau after 500 to 700 μm of crack growth.

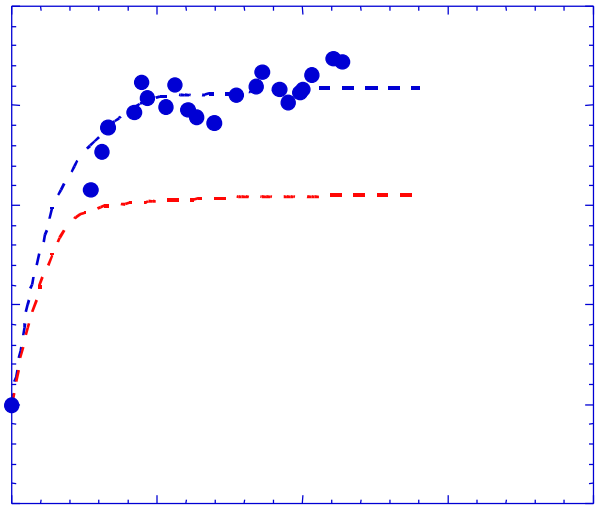

Fig. 2. Comparison of R-curves measured on 18 vol % samples with and without secondary heat treatment to remove residual Si.

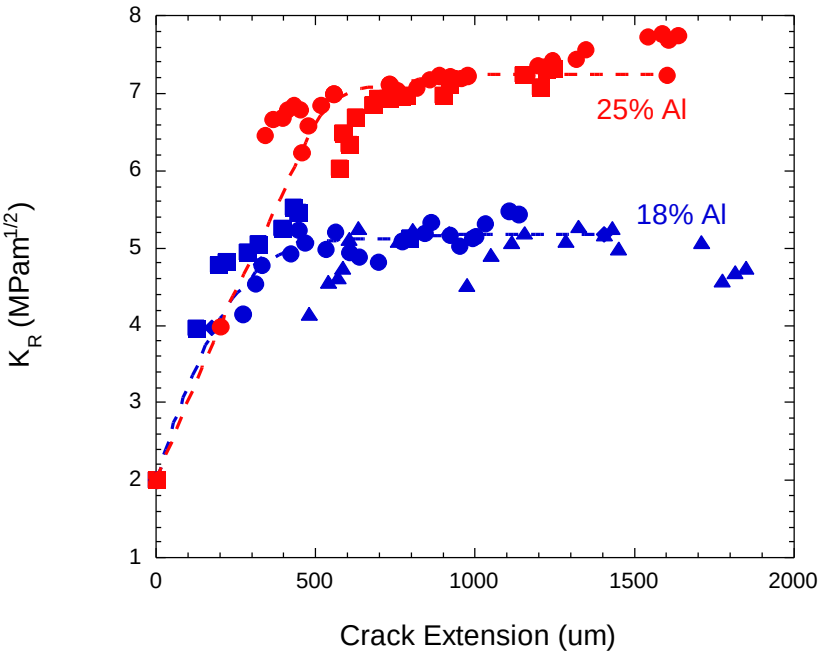

Fig. 3. Influence of metal content on the shape and plateau value of the R-curve.

We continued our measurements of the mechanical behavior of composites made from a variety of ceramic-metal and ceramic- intermetallic compositions. The new data are given as the bold entries in Table 1. The high bend strength of the Al_2O_3-Nb composite stands out. Like Al_2O_3-$MoSi_2$, the thermal expansions of the constituents of this system are closely matched. The result is a composite with low thermal stresses, which makes it ideal for applications requiring thermal cycling. Nb also is much more ductile than $MoSi_2$ at room temperature, making it ideal for applications that require high toughness. All of the experimental values of modulus are within measurement error of values predicted by a rule-of-mixture calculation using the modulus and volume fractions of each component.

Impact and future work. All of the materials for which R-curves were measured showed relatively steep slopes, which may enhance the reliability of these materials. Currently, we are measuring the strengths of enough samples for a statistical estimate of their reliability and to determine if the R-curve behavior is correlated with composite flaw sensitivity.

Table 1. Density, Strength, and Modulus of RHP Composites.

Composition	Density (g/cm^3)	Relative density (%)	Strength (MPa)	Young's Modulus (GPa)
Al_2O_3-Nb	5.38	97	524	
Al_2O_3-Ni	5.53	90	610	292
Al_2O_3-$MoSi_2$ (20%)	4.22	96	467	395
Al_2O_3-$MoSi_2$ (30%)	4.47	97	313	353
Al_2O_3-$Mo(Si,Al)_2$	4.39	95	240	320

Task 4: Development of commercial collaborations

As mentioned above, our detailed understanding of metal-ceramic reactions is applicable to improving the performance of refractories used in the metals-processing industry. For most of the work discussed here, we desire reactions to be extensive and rapid to make the composites of interest. However, we can take the opposite view and consider what conditions make ceramics most resistant to attack by molten metals. This is precisely the information of interest to refractories manufacturers who produce the products used to line kilns and furnaces such as those used in the aluminum industry. In FY 1997 we negotiated a three-way CRADA among Sandia, the Reynolds Metals Co., and the A. P. Green Co. in the area of improved refractories for aluminum reprocessing. Those discussions were suspended when we learned that the part of Reynolds we were dealing with had been sold and all of our contacts were leaving the company. Since that time we have had extensive discussions on an R&D collaboration with National Refractories and Minerals Corporation, located in Livermore, California. National is a major supplier of

refractories to the aluminum industry. We have signed a nondisclosure agreement with them and have done much of the preliminary work to establish a CRADA, which we expect to be in place in the first few months of calendar 1999. National already has begun preparing test specimens that will be evaluated in our laboratory as part of the collaborative work.

Recently we signed a nondisclosure agreement with BFD, Inc., of Columbus, Ohio, to exchange information on the ceramic-metal composites they are developing. BFD is a small company that has a patented method for making ceramic-metal composites that may have commercial potential as structural materials. We have discussed using our understanding of reaction mechanisms to answer some unresolved issues in the processing of the BFD composites.

SRI has pursued a number of collaborations for developing commercial applications of their composite coating. They have held discussions with various industrial representatives regarding testing of technology coatings and possible applications. SRI's spin-off company, 4C Technologies, is actively marketing their technology to industry. Four companies already have established small evaluation projects for assessing the coating technology in the following fields of use:

1. Ambient temperature–cured paints for construction and heavy industry (the second phase will start in 1999)
2. Paints for maintenance
3. Water-valve coatings
4. Oxidation-resistant coatings on ceramic composite.

A fifth coating project related to coating high-temperature components for aerospace applications is currently being discussed.

Task 5: Protective composite coatings on metals (summary of SRI results)

SRI is developing a low-cost approach to paints based on combining preceramic polymers and inorganic powder fillers. The base polymer is polyhydridomethylsiloxane (PHMS), a very low cost by-product of the silicone industry. This polymer can be modified or cured by a transition-metal catalytic approach developed at SRI. The powder fillers can be inert (e.g., TiO_2, SiO_2, and Al_2O_3) or active (e.g., Al and Zn). The active fillers also passivate the coatings. Curing at room temperature is being developed by first modifying the PHMS to convert all or part of the Si-H groups to Si-OH and Si-OR by catalytic dehydrocoupling reactions. The coating is further cured by hydrolysis-condensation using various acid and base catalysts.

This year SRI focused on improving formulations using modified polymers in which 5 to 20% of the Si-H bonds were replaced with RO- (R= Et, Pr, Bu, and benzyl), and the rest were substituted with Si-OH. A variety of mixed fillers were tested. Combinations of Al/Al_2O_3, Zn/SiO_2, and TiO_2/Al_2O_3, were found particularly interesting because of their

combined corrosion resistance and hardness. Room-temperature curing was achieved using various amines as hydrolysis-condensation or condensation catalysts. The cure rate was slowed to improve the bonding to the surface. Chemical surface treatments also were assessed to improve the bonding of the coatings to steel. A simple wash of the surface with 5% HNO_3 solution was found most effective, improving the interface bonding and consequently the corrosion resistance. Some surface-treated coatings passed over 1000 h of salt spray test and had hardness of 6H to 9H.

Impact. Preceramic polymer-based composite coatings are aimed at low-cost and simple protective coatings that will surpass the performance of paints currently used in heavy industry. Improved performance will allow the use of low-cost metals in harsh environments and at the same time reduce maintenance and costly shutdowns of plants.

Future work. SRI will continue improving room-temperature curing and will assess factors that affect the bonding of coatings to the surface. They will optimize formulations, generate performance data for corrosion-resistant coatings, and modify preceramic polymers to adjust shelf stability of paints and flexibility of cured coatings. SRI will evaluate characteristics and performance of high-temperature coatings in order to optimize formulations for high-temperature applications.

PUBLICATIONS

Journals

W. G. Fahrenholtz, K. G. Ewsuk, R. E. Loehman, and P. Lu, "Kinetics of Ceramic-Metal Composite Formation by Reactive Metal Penetration," *J. Amer. Ceram. Soc.* **81**(10), 2533–41 (1998).

P. Lu, T. B. Du, R. E. Loehman, K. G. Ewsuk, and W. G. Fahrenholtz, "Interfacial Microstructure Formed by Reactive Metal Penetration of Al into Mullite" (submitted).

W. G. Fahrenholtz, D. T. Ellerby, K. G. Ewsuk, and R. E. Loehman "Calculation and Control of Compositions of Al_2O_3-Al Composites by Reactive Metal Penetration of Dense Aluminosilicate Preforms" (submitted).

W. G. Fahrenholtz, B. P. Hansen, K. G. Ewsuk, and R. E. Loehman, "Forming Al_2O_3-Al-Si Composites by Combined Physical Infiltration and Reactive Metal Penetration of Porous Aluminosilicate Preforms" (submitted).

Proceedings

W. G. Fahrenholtz, K. G. Ewsuk, and R. E. Loehman, "Reactive Processing, Microstructure, and Mechanical Properties of Al_2O_3-$MoSi_2$ Composites," accepted for publication in *Proceedings of the 22nd Annual Cocoa Beach Conference on Composites, Advanced Ceramics, Materials, and Structures*, January 20–24, 1998.

Presentations

Oral presentations

R. E. Loehman, K. G. Ewsuk, W. G. Fahrenholtz, and J. J. Walker, "Chemical Effects in the Wetting of Ceramics by Molten Metals," presented at the Pacific Coast Regional and Basic Science Division Meetings of the American Ceramic Society, San Francisco, California, October 12–15, 1997.

W. G. Fahrenholtz, K. G. Ewsuk, and R. E. Loehman, "Processing and Properties of $MoSi_2$-Al_2O_3 Composites Formed by Reactive Hot Pressing," presented at the Pacific Coast Regional and Basic Science Division Meetings of the American Ceramic Society, San Francisco, California, October 12–15, 1997.

W. G. Fahrenholtz, "Ceramic-Metal and Ceramic- Intermetallic Composites Fabricated by Reactive Hot Pressing," presented at the Pacific Coast Regional and Basic Science Division Meetings of the American Ceramic Society, San Francisco, California, October 12–15, 1997.

J. J. Walker, W. G. Fahrenholtz, R. E. Loehman, and K. G. Ewsuk, "Wetting and Reaction Between Molten Aluminum Alloys and Oxide Ceramics," presented at the 9th Annual Symposium on Ceramics and Advanced Materials, Albuquerque, New Mexico, November 3, 1997.

E. Corral, D. T. Ellerby, W. G. Fahrenholtz, K. G. Ewsuk, and R. E. Loehman, "Processing and Characterizing Alumina-Aluminum Composites with Tailored Microstructures," presented at the 9th Annual Symposium on Ceramics and Advanced Materials, Albuquerque, New Mexico, November 3, 1997.

J. J. Walker, W. G. Fahrenholtz, K. G. Ewsuk, and R. E. Loehman, "Wetting and Reaction between Molten Al Alloys and Oxide Ceramics," presented at the 22nd Annual Cocoa Beach Conference on Composites, Advanced Ceramics, Materials, and Structures, January 20–24, 1998.

W. G. Fahrenholtz, K. G. Ewsuk, and R. E. Loehman, "Reactive Processing and Mechanical Properties of Alumina-Molybdenum Disilicide Composites," presented at the 22nd Annual Cocoa Beach Conference on Composites, Advanced Ceramics, Materials, and Structures, January 20–24, 1998.

W. G. Fahrenholtz, K. G. Ewsuk, and R. E. Loehman, "Fabrication of Ceramic-Metal and Ceramic-Intermetallic Composites by Reactive Hot Pressing," presented at the 100th Annual Meeting of the American Ceramic Society, May 3–6, 1998, Cincinnati, Ohio.

R. E. Loehman, W. G. Fahrenholtz, J. J. Walker, J. B. Davis, J. R. Porter, and P. E. D. Morgan, "Wetting and Reaction of Monazite by Al," presented at the 100th Annual Meeting of the American Ceramic Society, May 3–6, 1998, Cincinnati, Ohio.

D. T. Ellerby, R. Bordia, K. G. Ewsuk, R. E. Loehman, and W. G. Fahrenholtz, "Control of Al_2O_3/Al Composite Microstructure Using Reactive Metal Penetration," presented at

the 100th Annual Meeting of the American Ceramic Society, May 3–6, 1998, Cincinnati, Ohio.

D. T. Ellerby, R. Bordia, and J. Roedel, "Effect of Microstructure on the Toughening Behavior of Al_2O_3/Al Composites Using Reactive Metal Penetration," presented at the 100th Annual Meeting of the American Ceramic Society, May 3–6, 1998, Cincinnati, Ohio.

HONORS AND AWARDS

None.

PATENTS/DISCLOSURES

None.

LICENSES

None.

INDUSTRIAL INPUT, TECHNOLOGY TRANSFER, AND OTHER INTERACTIONS

Collaboration with Other Researchers

We are continuing our collaboration with A. P. Tomsia of Lawrence Berkeley National Laboratory (LBNL). Dr. Tomsia is the co-discoverer of reactive metal penetration and has contributed significantly in the past to its understanding and development. Dr. Eduardo Saiz is a visiting scientist working with Dr. Tomsia on the project and is supported by LBNL. Dr. Tomsia's participation is supported by internal funds from LBNL.

Professor Ping Lu of New Mexico Institute of Mining and Technology is supported on a subcontract to the project to provide TEM analysis of reaction zones and other structural information on reaction mechanisms. Professor Raj Bordia of the University of Washington has provided two graduate students, Don Ellerby and Erik Probsfield, who have been doing their thesis research at the Advanced Materials Laboratory during summers and in alternate semesters.

Dr. Sylvia Johnson and Dr. Yigal Blum have worked on a subcontract to the project to evaluate oxidation- and corrosion-resistant composite coatings on steel and Al. The coatings are made by full or partial pyrolysis of mixtures of organometallic polymers, metal powders, and ceramic additives, as described above.